arXiv:quant-ph/0104056v1 11 Apr 2001

Spontaneous Decay in the Presence of Absorbing Media

Ho Trung Dung†, Ludwig Knöll, and Dirk-Gunnar Welsch

Theoretisch-Physikalisches Institut, Friedrich-Schiller-Universität Jena,
Max-Wien-Platz 1, D-07743 Jena, Germany

(April 11, 2001)

ABSTRACT

After giving a summary of the basic-theoretical concept of quantization of the electromagnetic field in the presence of dispersing and absorbing (macroscopic) bodies, their effect on spontaneous decay of an excited atom is studied. Various configurations such as bulk material, planar half space media, spherical cavities, and microspheres are considered. In particular, the influence of material absorption on the local-field correction, the decay rate, the line shift, and the emission pattern are examined. Further, the interplay between radiative losses and losses due to material absorption is analyzed. Finally, the possibility of generating entangled states of two atoms coupled by a microsphere-assisted field is discussed.

1 INTRODUCTION

Spontaneous emission of an excited atom is not an immutable property of the atom, but it sensitively depends on the photonic spectral density of states that are involved in the atomic transition at the chosen location of the atom. Already Purcell (1946) pointed out that spontaneous emission can be enhanced when the atom is inside a cavity and its transition is in resonance with a cavity mode. The opposite case of inhibition of spontaneous emission is also possible [Kleppner (1981)]. It is further well known that the decay process can even be reversed by strongly coupling the atom to a sufficiently sharp cavity-field mode, so that the emitted photon can be reabsorbed and reemitted. Obviously, the photonic density of states can be modified by the presence of macroscopic bodies, which, in the simplest case, change the boundary conditions for the electromagnetic field. For the last years, engineering periodic dielectric structures (photonic crystals) has been of increasing interest [John (1987); Yablonovich (1987); John *et al.* (1994); Kofman *et al.* (1994); Joannopoulous *et al.* (1995); Soukoulis (Ed., 1996); Woldeyohannes *et al.* (1999); Nikolopoulos *et al.* (2000); Zhu *et al.* (2000); Schriemer *et al.* (2001)].

It is worth noting that spontaneous emission may be regarded as being a basic process in the rapidly growing field of cavity quantum electrodynamics (QED), where strong (resonant) interactions of a single or a few atoms with a single or a few radiation-field modes formed by material bodies are studied. Cavity QED itself has offered novel possibilities of testing fundamental aspects of quantum physics, such as quantum nondemolition measurement, complementarity, and entanglement [for reviews, see, e.g., Hinds (1991); Haroche (1992); Meschede (1992); Meystre (1992); Berman (Ed., 1994); Haroche (1998); Kimble (1998); Walther (1998)].

Spontaneous emission in the presence of material bodies is not only interesting from the point of view of fundamental research, but it has also offered a number of interesting applications. It can provide a reliable and efficient single-photon source to be used in quantum information processing [De Martini *et al.* (1996), Kitson *et al.* (1998)]. The sensitivity to the ambient medium of resonance fluorescence is crucial in scanning near-field optical microscopy [Betzig *et al.* (1993); Kopelman *et al.* (1993); Bian *et al.* (1995); Henkel *et al.* (1998); Gersen *et al.* (2000)]. Another important potential application is the so-called thresholdless laser [De Martini *et al.* (1988); Yamamoto *et al.* (1993); Protsenko *et al.* (1999)]. In a conventional laser, only a small portion of the spontaneous emission is channeled into the lasing mode formed by the cavity mirrors, the rest being

---

[†] On leave from the Institute of Physics, National Center for Sciences and Technology, 1 Mac Dinh Chi Street, District 1, Ho Chi Minh City, Vietnam.

lost to the free space modes. In a microcavity, due to strongly modified emission pattern and enhanced emission rate, a large portion of spontaneously emitted photons is stored in the cavity resonance mode. Losses due to excitation of free-space modes are thus drastically reduced and ultralow threshold lasing can be achieved.

Controlling of the spontaneous decay also plays an important role in solid-state systems, where instead of atoms, quantum well or quantum dot excitons play the role of the emitters [Yokoyama *et al.* (Eds., 1995); Khitrova *et al.* (1999); Yamamoto *et al.* (2000)]. So, the improved directionality of the spontaneously emitted light could have dramatic impact on manufacture of high-efficient light-emitting diodes and displays [Yamamoto *et al.* (1993)], and the spectral narrowing could help to increase the transmission capacity of optical fiber systems where chromatic dispersion is the limiting factor [Hunt *et al.* (1993)].

Although certain properties of spontaneous emission such as the decay rate can be described classically, using the model of a classically oscillating dipole interacting with its own radiation field [Chance *et al.* (1978); Wylie *et al.* (1985); Haroche (1992)], spontaneous emission is an intrinsically quantum mechanical process. Its proper description requires quantization of both the atom and the radiation field. Obviously, in the presence of material bodies the medium-assisted electromagnetic field must be quantized. As long as the medium can be regarded as being nondispersing and nonabsorbing, whose (real) permittivity changes with space in general, electromagnetic-field quantization can be performed, using, e.g., generalized orthogonal-mode expansion [Knöll *et al.* (1992)]. However, the concept fails when material absorption is included and the (spatially varying) permittivity becomes a complex function of frequency. The systematic study of the problem during the last years has generalized earlier results and offered powerful methods to deal with the special requirements of quantizing the electromagnetic field in absorbing media [for a review, see Knöll *et al.* (2001)].

There are many reasons why inclusion of material absorption in the study of spontaneous emission is desired. One might ask what would happen when the atomic transition frequency becomes close to a medium resonance, where absorption is strong. In particular the question of the effect of absorption on spontaneous emission in the presence of band-gap material arises. Obviously, spontaneous decay must not necessarily be accompanied by a really observable photon, if the atom is near an absorbing body, and the question is of what is the (average) fraction of emitted light. Another question is of how can absorption modify the local field felt by the atom. A rigorous approach to the problem has acquired even more significance with the recent progress in designing certain types of microcavities (e.g., microspheres), where the ultimate quality level determined by intrinsic material losses has been achieved [Gorodetsky *et al.* (1996)].

Although there has been a large body of theoretical work on medium-assisted spontaneous emission, material absorption has been ignored usually. Roughly speaking, there have been two concepts to treat absorption, namely the microscopic and the macroscopic approach. The microscopic approach starts from a microscopic model of the medium [Lee *et al.* (1995); Yeung *et al.* (1996); Juzeliūnas (1997); Fleischhauer (1999); Crenshaw *et al.* (2000a,b); Wubs *et al.* (2001)]. Accordingly, the underlying total Hamiltonian typically consists of the Hamiltonians of the free atom, the free radiation field, the atomic systems of the medium, and all the mutual interactions. The resulting equations of motion for the coupled system are then tried to rewrite in order to eliminate, on applying various approximation schemes, the medium variables and to obtain closed equations of motion for the atom-field system only. In this way, the life time of an excited atom in absorbing bulk material [Lee *et al.* (1995); Juzeliūnas (1997); Fleischhauer (1999); Crenshaw *et al.* (2000a,b); Wubs *et al.* (2001)], the initial transient regime [Wubs *et al.* (2001)], and the problem of local field corrections [Juzeliūnas (1997); Fleischhauer (1999); Crenshaw *et al.* (2000a,b); Wubs *et al.* (2001)] have been studied, and the problem of spontaneous emission of an excited atom near an absorbing interface has been considered [Yeung *et al.* (1996)]. The concepts typically borrow, at some stage of calculation, from macroscopic electrodynamics, e.g., when a (model-specific) permittivity is introduced, boundary conditions at surfaces of discontinuity are set or local-field corrections within the framework of cavity models are considered. Apart from the fact that the (simplified) microscopic models do not yield, in general, the exact permittivities, the calculations can become rather involved, particularly when surfaces of discontinuity are taken into account [Yeung *et al.* (1996)]. Further, the elimination of the medium variables must be done very carefully in order to ensure that the equal-time commutation relations are preserved. If this is not the case [Crenshaw *et al.* (2000a,b)], the results are questionable.

In the macroscopic approach, the medium is described, from the very beginning, in terms of a spatially varying permittivity, which is a complex function of frequency, $\varepsilon(\mathbf{r},\omega)$, that satisfies the Kramers–Kronig relations. This approach has – similar to classical optics – the benefit of being universally valid, because it uses only general physical properties, without the need of involved *ab initio* calculations. Clearly, this concept is valid only to some approximately fixed length scale which exceeds the average distance of two atoms. With regard to the calculation of the lifetimes and line shifts, the macroscopic approach is simple. It is well known that, according to Fermi's golden rule, the rate of spontaneous decay Γ of an excited atom [position $\mathbf{r}_A$, (real) transition dipole moment $\mathbf{d}$, transition frequency ω_A] can be expressed in terms of an electric-field correlation function as follows [see, e.g., Loudon (1983)]:

$$\Gamma = \frac{2\pi}{\hbar^2}\int_0^\infty \mathrm{d}\omega\, \langle 0|\mathbf{d}\hat{\mathbf{E}}(\mathbf{r}_\mathrm{A},\omega)\otimes\hat{\mathbf{E}}^\dagger(\mathbf{r}_\mathrm{A},\omega_\mathrm{A})\mathbf{d}|0\rangle \quad (1.1)$$

[cf. Eqs. (2.1) – (2.3)]. It is also well known [see, e.g., Abrikosov *et al.* (1975)] that, in agreement with the dissipation-fluctuation theorem, the relation

$$\langle 0|\hat{\boldsymbol{E}}(\mathbf{r},\omega)\otimes\hat{\boldsymbol{E}}^\dagger(\mathbf{r}',\omega')|0\rangle = \frac{\hbar\omega^2}{\pi\epsilon_0 c^2}\,\mathrm{Im}\,\boldsymbol{G}(\mathbf{r},\mathbf{r}',\omega)\,\delta(\omega-\omega') \quad (1.2)$$

(c, vacuum velocity of light) is valid, where $\boldsymbol{G}(\mathbf{r},\mathbf{r}',\omega)$ is the Green tensor of the classical, macroscopic Maxwell equations. Combining Eqs. (1.1) and (1.2) yields

$$\Gamma = \frac{2\omega_\mathrm{A}^2}{\hbar\varepsilon_0 c^2}\,\mathbf{d}\,\mathrm{Im}\,\boldsymbol{G}(\mathbf{r}_\mathrm{A},\mathbf{r}_\mathrm{A},\omega_\mathrm{A})\,\mathbf{d} \quad (1.3)$$

[see also Agarwal (1975); Wylie *et al.* (1984, 1985)]. The line shift can be calculated in a similar way to obtain

$$\delta\omega_A = \frac{\mathcal{P}}{\pi\hbar\varepsilon_0}\int_0^\infty \mathrm{d}\omega\,\frac{\omega^2}{c^2}\frac{\mathbf{d}\,\mathrm{Im}\,\boldsymbol{G}(\mathbf{r}_A,\mathbf{r}_A,\omega)\,\mathbf{d}}{\omega-\omega_A} \quad (1.4)$$

[$\mathcal{P}$, principal value; for a more rigorous derivation of Eqs. (1.3) and (1.4), see Section 3.2.1].

Hence, knowing the Green tensor of the classical problem for given complex permittivity, the decay rate and the line shift are known as well. Equations (1.3) and (1.4) were used in order to calculate decay rates and line shifts for an excited atom near a realistic (i.e., absorbing) metallic sphere [Ruppin (1982); Agarwal *et al.* (1983)], near an absorbing interface [Agarwal (1975); Agarwal *et al.* (1977); Wylie *et al.* (1984, 1985)], and in a planar cavity filled with an absorbing medium [Tomaš *et al.* (1999)]. Based on Eq. (1.3), spontaneous emission of an excited atom in absorbing bulk material was studied [Barnett *et al.* (1992)], including local field corrections [Barnett *et al.* (1996)]. The associated line shift (without local-field correction) was considered in Welton's interpretation [Matloob (2000)]. Spontaneous decay of an atom at the center of an absorbing sphere has been calculated in Tomaš (2001) (with local field correction).

In what follows we restrict our attention to the macroscopic approach that is based on QED in dispersing and absorbing media, within the framework of a source-quantity representation of the electromagnetic field in terms of the (classical) Green tensor of the macroscopic Maxwell equations and appropriately chosen fundamental bosonic fields [Huttner *et al.* (1992); Ho *et al.* (1993); Matloob *et al.* (1995); Gruner *et al.* (1996); Ho *et al.* (1998); Scheel *et al.* (1998); Knöll *et al.* (2001)]. The quantization scheme is outlined in Section 2. In Section 3, the basic formulas for studying the spontaneous decay of an excited atom are given, which cover both the strong- and the weak-coupling regime. Section 4 is devoted to the spontaneous decay in bulk material, with special emphasis on local-field effects. The problem of spontaneous decay near a planar interface is considered in Section 5, and Sections 6 and 7, respectively, present results for an atom in a spherical cavity and near a microsphere. In Section 8 a system of two atoms coupled to a microsphere is analyzed, with special emphasis on entangled-state preparation. Finally, a summary is given in Section 9.

2 QUANTIZATION SCHEME

Following Ho *et al.* (1998); Scheel *et al.* (1998); Knöll *et al.* (2001), we first consider the electromagnetic field in the presence of dispersing and absorbing macroscopic bodies in the case where no additional atomic sources are present. The electric-field operator $\hat{\mathbf{E}}$ can be represented in the form of

$$\hat{\mathbf{E}}(\mathbf{r}) = \hat{\mathbf{E}}^{(+)}(\mathbf{r}) + \hat{\mathbf{E}}^{(-)}(\mathbf{r}), \tag{2.1}$$

$$\hat{\mathbf{E}}^{(-)}(\mathbf{r}) = \left[\hat{\mathbf{E}}^{(+)}(\mathbf{r})\right]^{\dagger}, \tag{2.2}$$

$$\hat{\mathbf{E}}^{(+)}(\mathbf{r}) = \int_0^\infty \mathrm{d}\omega\, \underline{\hat{\mathbf{E}}}(\mathbf{r},\omega), \tag{2.3}$$

and the induction-field operator $\hat{\mathbf{B}}$ accordingly. The fields $\underline{\hat{\mathbf{E}}}$ and $\underline{\hat{\mathbf{B}}}$ then satisfy the macroscopic Maxwell equations

$$\boldsymbol{\nabla}\underline{\hat{\mathbf{B}}}(\mathbf{r},\omega) = 0, \tag{2.4}$$

$$\boldsymbol{\nabla}\left[\varepsilon_0\varepsilon(\mathbf{r},\omega)\underline{\hat{\mathbf{E}}}(\mathbf{r},\omega)\right] = \underline{\hat{\rho}}_{\mathrm{N}}(\mathbf{r},\omega), \tag{2.5}$$

$$\boldsymbol{\nabla}\times\underline{\hat{\mathbf{E}}}(\mathbf{r},\omega) = i\omega\underline{\hat{\mathbf{B}}}(\mathbf{r},\omega), \tag{2.6}$$

$$\boldsymbol{\nabla}\times\underline{\hat{\mathbf{B}}}(\mathbf{r},\omega) = \mu_0\underline{\hat{\mathbf{j}}}_{\mathrm{N}}(\mathbf{r},\omega) - \frac{i\omega}{c^2}\,\varepsilon(\mathbf{r},\omega)\underline{\hat{\mathbf{E}}}(\mathbf{r},\omega). \tag{2.7}$$

As already mentioned, the real part ε_R and the imaginary part ε_I of the complex (relative) permittivity $\varepsilon(\mathbf{r},\omega)$ satisfy (for any $\mathbf{r}$) the Kramers–Kronig relations. The operator noise charge and current densities $\underline{\hat{\rho}}_{\mathrm{N}}(\mathbf{r},\omega)$ and $\underline{\hat{\mathbf{j}}}_{\mathrm{N}}(\mathbf{r},\omega)$ respectively, which are associated with absorption, are related to the operator noise polarization $\underline{\hat{\mathbf{P}}}_{\mathrm{N}}(\mathbf{r},\omega)$ as

$$\underline{\hat{\rho}}_{\mathrm{N}}(\mathbf{r},\omega) = -\boldsymbol{\nabla}\underline{\hat{\mathbf{P}}}_{\mathrm{N}}(\mathbf{r},\omega), \tag{2.8}$$

$$\underline{\hat{\mathbf{j}}}_{\mathrm{N}}(\mathbf{r},\omega) = -i\omega\underline{\hat{\mathbf{P}}}_{\mathrm{N}}(\mathbf{r},\omega), \tag{2.9}$$

where

$$\underline{\hat{\mathbf{P}}}_{\mathrm{N}}(\mathbf{r},\omega) = i\sqrt{\frac{\hbar\varepsilon_0}{\pi}\varepsilon_I(\mathbf{r},\omega)}\,\hat{\mathbf{f}}(\mathbf{r},\omega). \tag{2.10}$$

Here, $\hat{\mathbf{f}}(\mathbf{r},\omega)$ and $\hat{\mathbf{f}}^{\dagger}(\mathbf{r},\omega)$ are bosonic fields which play the role of the fundamental variables of the composed system (electromagnetic field and medium including a dissipative system),

$$\left[\hat{f}_i(\mathbf{r},\omega), \hat{f}_j^{\dagger}(\mathbf{r}',\omega')\right] = \delta_{ij}\delta(\mathbf{r}-\mathbf{r}')\delta(\omega-\omega'), \tag{2.11}$$

$$\left[\hat{f}_i(\mathbf{r},\omega), \hat{f}_j(\mathbf{r}',\omega')\right] = 0. \tag{2.12}$$

From Eqs. (2.4) – (2.10) it follows that $\underline{\hat{\mathbf{E}}}$ can be written in the form

$$\begin{aligned}\underline{\hat{\mathbf{E}}}(\mathbf{r},\omega) = {} & i\sqrt{\frac{\hbar}{\pi\varepsilon_0}}\,\frac{\omega^2}{c^2}\\ & \times\int \mathrm{d}^3\mathbf{r}'\sqrt{\varepsilon_I(\mathbf{r}',\omega)}\,\boldsymbol{G}(\mathbf{r},\mathbf{r}',\omega)\hat{\mathbf{f}}(\mathbf{r}',\omega),\end{aligned} \tag{2.13}$$

and $\underline{\hat{\mathbf{B}}} = (i\omega)^{-1}\boldsymbol{\nabla}\times\underline{\hat{\mathbf{E}}}$ accordingly, where $\boldsymbol{G}(\mathbf{r},\mathbf{r}',\omega)$ is the classical Green tensor satisfying the equation

$$\left[\frac{\omega^2}{c^2}\,\varepsilon(\mathbf{r},\omega) - \boldsymbol{\nabla}\times\boldsymbol{\nabla}\times\right]\boldsymbol{G}(\mathbf{r},\mathbf{r}',\omega) = -\boldsymbol{\delta}(\mathbf{r}-\mathbf{r}') \tag{2.14}$$

together with the boundary condition at infinity [$\boldsymbol{\delta}(\mathbf{r})$, dyadic δ-function]. In this way, the electric field and the induction field are expressed in terms of a continuum set of the bosonic fields $\hat{\mathbf{f}}(\mathbf{r},\omega)$ [and $\hat{\mathbf{f}}^{\dagger}(\mathbf{r},\omega)$], and the Hamiltonian of the composed system reads (without the infinite ground-state energy)

$$\hat{H} = \int \mathrm{d}^3\mathbf{r}\int_0^\infty \mathrm{d}\omega\,\hbar\omega\,\hat{\mathbf{f}}^{\dagger}(\mathbf{r},\omega)\hat{\mathbf{f}}(\mathbf{r},\omega). \tag{2.15}$$

Using Eq. (2.13) [together with Eqs. (2.1) and (2.3)], one can introduce scalar and vector potentials $\hat{\varphi}$ and $\hat{\mathbf{A}}$, respectively, and express them in terms of the fundamental bosonic fields. In particular, in the Coulomb gauge one obtains

$$-\boldsymbol{\nabla}\hat{\varphi}(\mathbf{r}) = \hat{\mathbf{E}}^{\|}(\mathbf{r}), \tag{2.16}$$

$$\hat{\mathbf{A}}(\mathbf{r}) = \int_0^\infty \mathrm{d}\omega\,(i\omega)^{-1}\underline{\hat{\mathbf{E}}}^{\perp}(\mathbf{r},\omega) + \mathrm{H.c.}, \tag{2.17}$$

where

$$\hat{\mathbf{E}}^{\perp(\|)}(\mathbf{r}) = \int \mathrm{d}^3\mathbf{r}'\,\boldsymbol{\delta}^{\perp(\|)}(\mathbf{r}-\mathbf{r}')\,\hat{\mathbf{E}}(\mathbf{r}'), \tag{2.18}$$

with $\boldsymbol{\delta}^{\perp}(\mathbf{r})$ and $\boldsymbol{\delta}^{\|}(\mathbf{r})$ being the dyadic transverse and longitudinal δ-functions, respectively.

We now consider the interaction of the medium-assisted electromagnetic field with additional point charges q_α. Applying the minimal-coupling scheme, we may write the complete Hamiltonian in the form of

$$\begin{aligned}\hat{H} = {} & \int \mathrm{d}^3\mathbf{r}\int_0^\infty \mathrm{d}\omega\,\hbar\omega\,\hat{\mathbf{f}}^{\dagger}(\mathbf{r},\omega)\hat{\mathbf{f}}(\mathbf{r},\omega)\\ & + \sum_\alpha \frac{1}{2m_\alpha}\left[\hat{\mathbf{p}}_\alpha - q_\alpha\hat{\mathbf{A}}(\hat{\mathbf{r}}_\alpha)\right]^2\\ & + \tfrac{1}{2}\int \mathrm{d}^3\mathbf{r}\,\hat{\rho}_A(\mathbf{r})\hat{\varphi}_A(\mathbf{r}) + \int \mathrm{d}^3\mathbf{r}\,\hat{\rho}_A(\mathbf{r})\hat{\varphi}(\mathbf{r}),\end{aligned} \tag{2.19}$$

where $\hat{\mathbf{r}}_\alpha$ is the position operator and $\hat{\mathbf{p}}_\alpha$ is the canonical momentum operator of the αth charged particle of mass m_α. The Hamiltonian (2.19) consists of four terms. The first term is the energy observed when the particles are absent [cf. Eq. (2.15)]. The second term is the kinetic energy of the particles, and the third and fourth terms are their Coulomb energies, where the potential $\hat{\varphi}_A$ can be given by

$$\hat{\varphi}_A(\mathbf{r}) = \int \mathrm{d}^3\mathbf{r}'\,\frac{\hat{\rho}_A(\mathbf{r}')}{4\pi\varepsilon_0|\mathbf{r}-\mathbf{r}'|}\,, \tag{2.20}$$

with

$$\hat{\rho}_A(\mathbf{r}) = \sum_\alpha q_\alpha\delta(\mathbf{r}-\hat{\mathbf{r}}_\alpha) \tag{2.21}$$

being the charge density. Obviously, the last term in Eq. (2.19) is the Coulomb energy of interaction of the particles with the medium. Note that all terms are expressed in terms of the dynamical variables $\hat{\mathbf{f}}(\mathbf{r},\omega)$, $\hat{\mathbf{f}}^\dagger(\mathbf{r},\omega)$, $\hat{\mathbf{r}}_\alpha$, and $\hat{\mathbf{p}}_\alpha$. It is worth noting the quantization scheme is fully equivalent to the so-called auxiliary-field scheme introduced by Tip (1998) [for details, see Tip *et al.* (2001)].

3 SPONTANEOUS DECAY: GENERAL FORMALISM

3.1 Basic equations

Let us consider N two-level atoms [positions $\mathbf{r}_A$, transition frequencies ω_A $(A=1,2,...,N)$] that resonantly interact with radiation via electric-dipole transition (dipole moments $\mathbf{d}_A$). Let us further assume that the atoms are sufficiently far from each other, so that the interatom Coulomb interaction can be ignored. In this case, the electric-dipole approximation and the rotating wave approximation apply, and the minimal-coupling Hamiltonian takes the form of [Ho *et al.* (2000); Knöll *et al.* (2001)]

$$\hat{H} = \int \mathrm{d}^3\mathbf{r} \int_0^\infty \mathrm{d}\omega\, \hbar\omega\, \hat{\mathbf{f}}^\dagger(\mathbf{r},\omega)\hat{\mathbf{f}}(\mathbf{r},\omega) + \sum_A \tfrac{1}{2}\hbar\omega_A\hat{\sigma}_{Az} - \sum_A \left[\hat{\sigma}_A^\dagger \hat{\mathbf{E}}^{(+)}(\mathbf{r}_A)\mathbf{d}_A + \mathrm{H.c.}\right]. \quad (3.1)$$

Here and in the following, the two-level atoms are described in terms of the Pauli operators $\hat{\sigma}_A$, $\hat{\sigma}_A^\dagger$, and $\hat{\sigma}_{Az}$.

For a single-quantum excitation of the system, the system wave function at time t can be written as

$$|\psi(t)\rangle = \sum_A C_{U_A}(t) e^{-i(\omega_A-\bar{\omega})t}|U_A\rangle|\{0\}\rangle + \int \mathrm{d}^3\mathbf{r} \int_0^\infty \mathrm{d}\omega \left[C_{Li}(\mathbf{r},\omega,t) \times e^{-i(\omega-\bar{\omega})t}|L\rangle|\{1_i(\mathbf{r},\omega)\}\rangle\right] \quad (3.2)$$

($\bar{\omega} = \frac{1}{2}\sum_A \omega_A$). Here, $|U_A\rangle$ is the excited atomic state, where the Ath atom is in the upper state and all the other atoms are in the lower state, and $|L\rangle$ is the atomic state, where all atoms are in the lower state. Accordingly, $|\{0\}\rangle$ is the vacuum state of the rest of the system, and $|\{1_i(\mathbf{r},\omega)\}\rangle$ is the state, where it is excited in a single-quantum Fock state. The Schrödinger equation yields

$$\dot{C}_{U_A}(t) = \frac{-1}{\sqrt{\pi\varepsilon_0\hbar}} \int_0^\infty \mathrm{d}\omega \int \mathrm{d}^3\mathbf{r} \left\{ \frac{\omega^2}{c^2}\, e^{-i(\omega-\omega_A)t} \times \left[\sqrt{\varepsilon_I(\mathbf{r},\omega)}\, \mathbf{d}_A \boldsymbol{G}(\mathbf{r}_A,\mathbf{r},\omega)\mathbf{C}_L(\mathbf{r},\omega,t)\right]\right\}, \quad (3.3)$$

$$\dot{\mathbf{C}}_L(\mathbf{r},\omega,t) = \sum_A \frac{1}{\sqrt{\pi\varepsilon_0\hbar}} \frac{\omega^2}{c^2}\, e^{i(\omega-\omega_A)t} \times \sqrt{\varepsilon_I(\mathbf{r},\omega)}\mathbf{d}_A \boldsymbol{G}^*(\mathbf{r}_A,\mathbf{r},\omega)\, C_{U_A}(t). \quad (3.4)$$

We now substitute the result of formal integration of Eq. (3.4) into Eq. (3.3). Making use of the relationship

$$\mathrm{Im}\, G_{ij}(\mathbf{r},\mathbf{r}',\omega) = \int \mathrm{d}^3\mathbf{s} \left[\frac{\omega^2}{c^2}\, \varepsilon_I(\mathbf{s},\omega) \times G_{ik}(\mathbf{r},\mathbf{s},\omega) G_{jk}^*(\mathbf{r}',\mathbf{s},\omega)\right], \quad (3.5)$$

we obtain the following (closed) system of integro-differential equations:

$$\dot{C}_{U_A}(t) = \sum_{A'} \int_0^t \mathrm{d}t'\, K_{AA'}(t,t')\, C_{U_{A'}}(t') - \frac{1}{\sqrt{\pi\varepsilon_0\hbar}} \int_0^\infty \mathrm{d}\omega \int \mathrm{d}^3\mathbf{r} \left\{ \frac{\omega^2}{c^2}\, e^{-i(\omega-\omega_A)t} \times \left[\sqrt{\varepsilon_I(\mathbf{r},\omega)}\, \mathbf{d}_A \boldsymbol{G}(\mathbf{r}_A,\mathbf{r},\omega)\mathbf{C}_L(\mathbf{r},\omega,0)\right]\right\}, \quad (3.6)$$

$$K_{AA'}(t,t') = \frac{-1}{\hbar\pi\varepsilon_0} \int_0^\infty \mathrm{d}\omega \left[\frac{\omega^2}{c^2} e^{-i(\omega-\omega_A)t} \times e^{i(\omega-\omega_{A'})t'} \mathbf{d}_A \mathrm{Im}\, \boldsymbol{G}(\mathbf{r}_A,\mathbf{r}_{A'},\omega)\mathbf{d}_{A'}\right]. \quad (3.7)$$

Note that

$$K_{AA'}(t,t') = K_{A'A}^*(t',t), \quad (3.8)$$

because of the reciprocity theorem.

The excitation can initially reside in either an atom or the medium-assisted electromagnetic field. The latter case, i.e., $\mathbf{C}_L(\mathbf{r},\omega,0)\neq 0$ in Eq. (3.6), could be realized, for example, by coupling the field first to an excited atom D in a time interval Δt such that, according to Eq. (3.4), $\mathbf{C}_L(\mathbf{r},\omega,0)$ reads

$$\mathbf{C}_L(\mathbf{r},\omega,0) = \int_{-\Delta t}^0 \mathrm{d}t' \frac{1}{\sqrt{\pi\varepsilon_0\hbar}} \frac{\omega^2}{c^2}\, e^{i(\omega-\omega_D)t'} \times \sqrt{\varepsilon_I(\mathbf{r},\omega)}\mathbf{d}_D \boldsymbol{G}^*(\mathbf{r}_D,\mathbf{r},\omega)\, C_{U_D}(t'), \quad (3.9)$$

where $C_{U_D}(t)$ describes the single-atom decay according to Eq. (3.13) given below. Substitution of the expression (3.9) into Eq. (3.6) then yields

$$\dot{C}_{U_A}(t) = \sum_{A'} \int_0^t \mathrm{d}t'\, K_{AA'}(t,t')\, C_{U_{A'}}(t') + \int_{-\Delta t}^0 \mathrm{d}t'\, K_{AD}(t,t')\, C_{U_D}(t'). \tag{3.10}$$

3.2 Single-Atom Decay

3.2.1 Atomic Dynamics

Let us restrict our attention to the spontaneous decay of a single atom. For the initial condition $\mathbf{C}_L(\mathbf{r},\omega,0)=0$, Eq. (3.6) becomes ($C_U \equiv C_{U_A}$, $\mathbf{d}\equiv\mathbf{d}_A$)

$$\dot{C}_U(t) = \int_0^t \mathrm{d}t'\, K(t-t')C_U(t'), \tag{3.11}$$

where

$$K(t-t') = K_{AA}(t,t'). \tag{3.12}$$

Integrating both sides of Eq. (3.11) with respect to time, we easily derive, on changing the order of integrations on the right-hand side, a Volterra integral equation of the second kind,

$$C_U(t) = \int_0^t \mathrm{d}t'\, \bar{K}(t-t')C_U(t') + 1 \tag{3.13}$$

[$C_U(0)=1$], where, according to Eqs. (3.12) and (3.7),

$$\bar{K}(t-t') = \frac{-1}{\hbar\pi\varepsilon_0}\int_0^\infty \mathrm{d}\omega \biggl\{\Bigl[1-e^{-i(\omega-\omega_A)(t-t')}\Bigr] \times \frac{\omega^2}{c^2}\,\frac{\mathbf{d}\mathrm{Im}\,\boldsymbol{G}(\mathbf{r}_A,\mathbf{r}_A,\omega)\mathbf{d}}{i(\omega-\omega_A)}\biggr\}. \tag{3.14}$$

It is worth noting that Eqs. (3.11) and (3.13) apply to the spontaneous decay of an atom in the presence of an arbitrary configuration of dispersing and absorbing macroscopic bodies. All the matter parameters that are relevant for the atomic evolution are contained, via the Green tensor, in the kernel functions (3.12) and (3.14). In particular when absorption is disregarded and the permittivity is regarded as being a real, frequency-independent quantity (which of course can change with space), then the formalism yields the results of standard mode decomposition, obtained by Laplace transform techniques [Lewenstein *et al.* (1988a,b); John *et al.* (1994)] and delay-differential-equation techniques [Cook *et al.* (1987); Feng *et al.* (1989); Ho *et al.* (1999)]. It should be pointed out that the Green tensor has been available for a large variety of configurations such as planarly, spherically, and cylindrically multilayered media [Tai (1994); Chew (1995)].

In order to study the case where the atom is surrounded by matter, the atom should be assumed to be localized in some small free-space region, so that the Green tensor at the position of the atom reads

$$\boldsymbol{G}(\mathbf{r}_A,\mathbf{r}_A,\omega)=\boldsymbol{G}^V(\mathbf{r}_A,\mathbf{r}_A,\omega)+\boldsymbol{G}^R(\mathbf{r}_A,\mathbf{r}_A,\omega), \tag{3.15}$$

where $\boldsymbol{G}^V$ is the vacuum Green tensor with

$$\mathrm{Im}\,\boldsymbol{G}^V(\mathbf{r}_A,\mathbf{r}_A,\omega) = \frac{\omega}{6\pi c}\,\boldsymbol{I} \tag{3.16}$$

(Appendix A.1), and $\boldsymbol{G}^R$ describes the effects of reflections at the (surface of discontinuity of the) surrounding medium. The contribution of $\boldsymbol{G}^V$ to $\bar{K}$ in Eq. (3.14) can be treated in the Markov approximation (see below), thus

$$\bar{K}(t-t') = -\tfrac{1}{2}\Gamma_0 + \frac{1}{\hbar\pi\varepsilon_0}\int_0^\infty \mathrm{d}\omega\,\frac{\omega^2}{c^2} \times \frac{\mathbf{d}\mathrm{Im}\,\boldsymbol{G}^R(\mathbf{r}_A,\mathbf{r}_A,\omega)\mathbf{d}}{i(\omega-\omega_A)}\Bigl[e^{-i(\omega-\omega_A)(t-t')}-1\Bigr], \tag{3.17}$$

where Γ_0 is the well-known decay rate in free space,

$$\Gamma_0 = \frac{\omega_A^3 d^2}{3\hbar\pi\varepsilon_0 c^3}\,. \tag{3.18}$$

The integro-differential equation (3.11) [or the integral equation (3.13)] together with the kernel function (3.12) [or (3.17)] can be regarded as the basic equation for studying the influence of an arbitrary configuration of dispersing and absorbing matter on the spontaneous decay of an excited atom.

Weak Coupling When the Markov approximation applies, i.e., when in a coarse-grained description of the atomic motion memory effects are disregarded, then we may let

$$\frac{e^{i(\omega_A-\omega)(t-t')}-1}{i(\omega_A-\omega)} \quad\to\quad \zeta(\omega_A-\omega) \tag{3.19}$$

in Eq. (3.14) [$\zeta(x)=\pi\delta(x)+i\mathcal{P}/x$], and thus

$$\bar{K}(t-t') = -\tfrac{1}{2}\Gamma + i\delta\omega_A, \tag{3.20}$$

where Γ and $\delta\omega_A$ are respectively given by Eqs. (1.3) and (1.4). Substitution of the expression (3.20) into

Eq. (3.13) for the kernel function yields the familiar (weak-coupling) result that

$$C_U(t) = \exp\left[\left(-\tfrac{1}{2}\Gamma + i\delta\omega_A\right) t\right]. \qquad (3.21)$$

Application of Eqs. (1.3), (1.4), (3.15), and (3.16) yields

$$\Gamma = \Gamma_0 + \frac{2\omega_A^2}{\hbar\varepsilon_0 c^2}\, \mathbf{d}\mathrm{Im}\, \boldsymbol{G}^R(\mathbf{r}_A, \mathbf{r}_A, \omega_A)\mathbf{d}, \qquad (3.22)$$

$$\delta\omega_A = \frac{\omega_A^2}{\hbar\varepsilon_0 c^2}\Bigg[\mathbf{d}\mathrm{Re}\, \boldsymbol{G}^R(\mathbf{r}_A, \mathbf{r}_A, \omega_A)\mathbf{d} - \frac{1}{\pi}\int_0^\infty \mathrm{d}\omega\, \frac{\omega^2}{\omega_A^2}\, \frac{\mathbf{d}\mathrm{Im}\, \boldsymbol{G}^R(\mathbf{r}_A, \mathbf{r}_A, \omega)\mathbf{d}}{\omega + \omega_A}\Bigg]. \qquad (3.23)$$

In Eq. (3.23), the Kramers–Kronig relations have been used and the divergent contribution of the vacuum to the line shift is thought of as being included in the atomic transition frequency ω_A. It is not difficult to see that in Eq. (3.23) the second term, which is only weakly sensitive to the atomic transition frequency, is small compared to the first one and can therefore be neglected in general.

Strong Coupling When the atomic transition frequency approaches a resonance frequency of a resonator-like equipment of macroscopic bodies, then the strength of the coupling between the atom and the electromagnetic field can increase to such an extent that the weak-coupling approximation fails and the integral equation (3.11) must be considered. Let us assume, for simplicity, that only a single (field-)resonance line of Lorentzian shape is involved in the atom–field interaction. In this case, the kernel function (3.12) may be approximated by

$$K(t-t') \simeq -\frac{\Gamma_C(\Delta\omega_C)^2}{2\pi} \mathrm{e}^{-i(\omega_C-\omega_A)(t-t')} \times \int_{-\infty}^{\infty} \mathrm{d}\omega\, \frac{\mathrm{e}^{-i(\omega-\omega_C)(t-t')}}{(\omega-\omega_C)^2 + (\Delta\omega_C)^2} = \tfrac{1}{2}\Gamma_C \Delta\omega_C \mathrm{e}^{-i(\omega_C-\omega_A)(t-t')} \mathrm{e}^{-\Delta\omega_C|t-t'|}, \qquad (3.24)$$

and thus the integral equation (3.11) corresponds to the differential equation [Ho *et al.* (2000)]

$$\ddot{C}_U(t) + \left[i(\omega_C - \omega_A) + \Delta\omega_C\right] \dot{C}_U(t) + \tfrac{1}{2}\Gamma_C \Delta\omega_C C_U(t) = 0. \qquad (3.25)$$

Here, ω_C and $\Delta\omega_C$ are respectively the mid-frequency and the line width of the field resonance associated with the bodies, and Γ_C is the (weak-coupling) decay rate at ω_C.

Equation (3.25) typically applies to the strong-coupling regime for an arbitrary resonator configuration, provided that the field that effectively interacts with the atom can be regarded as being a single-resonance field of Lorentzian shape.[1] In particular, when material absorption is disregarded, then the line broadening solely results from the radiative losses due to the input-output coupling [Cook *et al.* (1987); Lai *et al.* (1988); Feng *et al.* (1989)].

Equation (3.25) reveals that the upper-state probability amplitude of the atom obeys the equation of motion for a damped harmonic oscillator. In the strong-coupling regime, where $\omega_A = \omega_C$ and $\Omega \gg \Delta\omega_C$, damped Rabi oscillations are observed:

$$C_U(t) = \mathrm{e}^{-\Delta\omega_C t/2} \cos(\Omega t/2), \qquad (3.26)$$

where the Rabi frequency Ω reads

$$\Omega = \sqrt{2\Gamma_C \Delta\omega_C}\,. \qquad (3.27)$$

3.2.2 Emitted-Light Intensity

It is well known that the intensity of light registered by a point-like photodetector at position $\mathbf{r}$ and time t is given by

$$I(\mathbf{r}, t) \equiv \langle\psi(t)|\hat{\mathbf{E}}^{(-)}(\mathbf{r})\hat{\mathbf{E}}^{(+)}(\mathbf{r})|\psi(t)\rangle. \qquad (3.28)$$

The emitted-light intensity associated with the spontaneous decay of an excited atom in the presence of dispersing and absorbing matter can be obtained by combining Eqs. (2.1) – (2.3), (2.13), (3.2), and (3.5). The result is

$$I(\mathbf{r}, t) = \Bigg|\frac{\omega_A^2}{\pi\varepsilon_0 c^2} \int_0^t \mathrm{d}t' \int_0^\infty \mathrm{d}\omega \Big[C_U(t') \times e^{-i(\omega-\omega_A)(t-t')} \mathrm{Im}\, \boldsymbol{G}(\mathbf{r}, \mathbf{r}_A, \omega)\, \mathbf{d}\Big]\Bigg|^2, \qquad (3.29)$$

where, in the spirit of the rotating wave approximation used, $\omega^2 = \omega_A^2$ has been set in the frequency integral. Again, all relevant matter parameters are contained in the Green tensor. In contrast to Eq. (3.13) [together with the kernel function (3.17)], Eq. (3.29) requires information about the Green tensor at different space points. In particular, its dependence on space and frequency essentially determines the retardation effects.

---

[1] Equations of the type (3.25) can also be obtained within the framework of standard (Markovian) quantum noise theory, where an appropriately chosen undamped mode is coupled to a two-level atom and some reservoir [Sachdev (1984)].

In the simplest case of free space we have

$$\mathrm{Im}\,\boldsymbol{G}^{V}(\mathbf{r},\mathbf{r}_A,\omega)=\frac{1}{8i\pi\rho}\left(\boldsymbol{I}-\frac{\boldsymbol{\rho}\otimes\boldsymbol{\rho}}{\rho^2}\right) \times\left(e^{i\omega\rho/c}-e^{-i\omega\rho/c}\right)+\mathcal{O}\bigl(\rho^{-2}\bigr) \tag{3.30}$$

($\boldsymbol{\rho}=\mathbf{r}-\mathbf{r}_A$; Appendix A.1). We substitute Eqs. (3.21) ($\Gamma=\Gamma_0$) and (3.30) into Eq. (3.29), calculate the time integral, and extend the lower limit in the frequency integral to $-\infty$,

$$\int_{-\infty}^{\infty}\mathrm{d}\omega\left(e^{i\omega\rho/c}-e^{-i\omega\rho/c}\right)\frac{e^{-(\Gamma_0/2+i\omega_A')t}-e^{-i\omega t}}{i[\omega-(\omega_A'-i\Gamma_0/2)]} =-2\pi\exp\Bigl[\bigl(-\tfrac{1}{2}\Gamma_0-i\omega_A'\bigr)\Bigl(t-\frac{\rho}{c}\Bigr)\Bigr]\,\Theta\Bigl(t-\frac{\rho}{c}\Bigr) \tag{3.31}$$

[$\Theta(x)$, unit step function], where

$$\omega_A'=\omega_A-\delta\omega_A\,. \tag{3.32}$$

Thus, the well-known (far-field) result

$$I(\mathbf{r},t)=\left(\frac{\omega_A^2 d\sin\theta}{4\pi\varepsilon_0c^2\rho}\right)^2 e^{-\Gamma_0(t-\rho/c)}\,\Theta(t-\rho/c) \tag{3.33}$$

is recognized (θ, angle between $\boldsymbol{\rho}$ and $\boldsymbol{d}$).

It should be noted that the general expression (3.29) is valid for an arbitrary coupling regime. In particular, in the weak-coupling regime the Markov approximation applies, and $C_U(t')$ can be taken at $t'=t$ and put in front of the time integral in Eq. (3.29), with $C_U(t)$ being simply the exponential (3.21). Equation (3.29) thus simplifies to

$$I(\mathbf{r},t)\simeq|\mathbf{F}(\mathbf{r},\mathbf{r}_A,\omega_A)|^2e^{-\Gamma t}, \tag{3.34}$$

where

$$\mathbf{F}(\mathbf{r},\mathbf{r}_A,\omega_A)=-\frac{i\omega_A^2}{\varepsilon_0c^2}\biggl[\boldsymbol{G}(\mathbf{r},\mathbf{r}_A,\omega_A)\mathbf{d} -\frac{1}{\pi}\int_0^{\infty}\mathrm{d}\omega\,\frac{\mathrm{Im}\,\boldsymbol{G}(\mathbf{r},\mathbf{r}_A,\omega)\mathbf{d}}{\omega+\omega_A}\biggr]. \tag{3.35}$$

Since the second term on the right-hand side of Eq. (3.35) is small compared to the first one, it can be omitted, and the spatial distribution of the emitted-light intensity (emission pattern) can be given by, on disregarding transit time delay,

$$|\mathbf{F}(\mathbf{r},\mathbf{r}_A,\omega_A)|^2\simeq\left|\frac{\omega_A^2}{\varepsilon_0c^2}\,\boldsymbol{G}(\mathbf{r},\mathbf{r}_A,\omega_A)\mathbf{d}\right|^2. \tag{3.36}$$

Material absorption gives rise to nonradiative decay. The fraction of really emitted radiation energy can be obtained by integration of the Pointing-vector expectation value with respect to time and over the surface of a sphere whose radius r is much larger than the extension of the system consisting of the macroscopic bodies and the atom,

$$W=2c\varepsilon_0\int_0^{\infty}\mathrm{d}t\int_0^{2\pi}d\phi\int_0^{\pi}d\theta\,r^2\sin\theta\,I(\mathbf{r},t). \tag{3.37}$$

The ratio W/W_0 ($W_0=\hbar\omega_A$) then gives us a measure of the emitted radiation energy, and accordingly, $1-W/W_0$ measures the energy absorbed by the bodies.

3.2.3 Emitted-Light Spectrum

Next, let us consider the time-dependent power spectrum of the emitted light, which for sufficiently small passband width of the spectral apparatus can be given by [see, e.g., Vogel *et al.* (1994)]

$$S(\mathbf{r},\omega_S,T)=\int_0^T\mathrm{d}t_2\int_0^T\mathrm{d}t_1\Bigl[e^{-i\omega_S(t_2-t_1)} \times\bigl\langle\hat{\mathbf{E}}^{(-)}(\mathbf{r},t_2)\hat{\mathbf{E}}^{(+)}(\mathbf{r},t_1)\bigr\rangle\Bigr], \tag{3.38}$$

where ω_S is the setting frequency of the spectral apparatus and T is the operating-time interval of the detector. In close analogy to the derivation of Eq. (3.29), combination of Eqs. (2.1) – (2.3), (2.13), (3.2), and (3.5) leads to

$$S(\mathbf{r},\omega_S,T)=\biggl|\frac{\omega_A^2}{\pi\varepsilon_0c^2}\int_0^T\mathrm{d}t_1\Bigl[e^{i(\omega_S-\omega_A)t_1} \times\int_0^{t_1}\mathrm{d}t'\,C_U(t')\int_0^{\infty}\mathrm{d}\omega\,e^{-i(\omega-\omega_A)(t_1-t')} \times\mathrm{Im}\,\boldsymbol{G}(\mathbf{r},\mathbf{r}_A,\omega)\mathbf{d}\Bigr]\biggr|^2. \tag{3.39}$$

Further calculation again requires knowledge of the Green tensor of the problem.

Let us use Eq. (3.39) to recover the free-space result. Following the line that has led from Eq. (3.29) to Eq. (3.33), we find that

$$S(\mathbf{r},\omega_S,T)=\left(\frac{\omega_A^2 d\sin\theta}{4\pi\varepsilon_0c^2\rho}\right)^2\Theta(T-\rho/c) \times\left|\frac{e^{[-\Gamma_0/2+i(\omega_S-\omega_A')](T-\rho/c)}-1}{\omega_S-\omega_A'+i\Gamma_0/2}\right|^2. \tag{3.40}$$

In particular for $T\to\infty$, we recognize the well-known Lorentzian:

$$\lim_{T\to\infty} S(\mathbf{r},\omega_S,T) = \left(\frac{\omega_A^2 d\sin\theta}{4\pi\varepsilon_0 c^2\rho}\right)^2 \times \frac{1}{(\omega_S-\omega_A')^2+\Gamma_0^2/4}\,. \tag{3.41}$$

If retardation is ignored and the Markov approximation applies, Eq. (3.39) can be simplified in a similar way as Eq. (3.29). In close analogy to the derivation of Eq. (3.34) we may write

$$S(\mathbf{r},\omega_S,T) = |\mathbf{F}(\mathbf{r},\mathbf{r}_A,\omega_A)|^2 \times \left|\frac{e^{[-\Gamma/2+i(\omega_S-\omega_A')]T}-1}{\omega_S-\omega_A'+i\Gamma/2}\right|^2, \tag{3.42}$$

with $\mathbf{F}(\mathbf{r},\mathbf{r}_A,\omega_A)$ from Eq. (3.35).

3.3 Two-Atom Coupling

We now turn to the problem of two atoms (denoted by A and B) coupled through a medium-assisted electromagnetic field in the case of single-quantum excitation. For simplicity, let us consider atoms with equal transition frequencies, so that

$$K_{AA'}(t,t') \equiv K_{AA'}(t-t') \tag{3.43}$$

$(A'=B,D)$ and

$$K_{AB}(t-t') = K_{BA}(t-t'), \tag{3.44}$$

and assume that the isolated atoms undergo the same decay law,

$$K_{AA}(t,t') = K_{BB}(t,t') \equiv K(t-t'). \tag{3.45}$$

Introducing the new variables

$$C_\pm(t) = 2^{-1/2}\Big[C_{U_A}(t) \pm C_{U_B}(t)\Big], \tag{3.46}$$

it is not difficult to prove that the integro-differential equations (3.10) decouple as follows:

$$\dot{C}_\pm(t) = \int_0^t \mathrm{d}t'\, K_\pm(t-t')\, C_\pm(t') + 2^{-1/2}\int_{-\Delta t}^0 \mathrm{d}t'\,\big[K_{AD}(t-t') \pm K_{BD}(t-t')\big]\, C_{U_D}(t'), \tag{3.47}$$

where

$$K_\pm(t-t') = K(t-t') \pm K_{AB}(t-t'). \tag{3.48}$$

Obviously, the $C_\pm$ are the expansion coefficients of the wave function with respect to the (atomic) basis

$$|\pm\rangle = 2^{-1/2}\left(|U_A\rangle \pm |U_B\rangle\right), \tag{3.49}$$

and $|L\rangle$ (instead of the basis $|U_A\rangle$, $|U_B\rangle$, and $|L\rangle$). Thus, they are the probability amplitudes of finding the total system in the states $|+\rangle|\{0\}\rangle$ and $|-\rangle|\{0\}\rangle$, respectively. In the further treatment of Eq. (3.47) one can again distinguish between the weak- and the strong-coupling regime.

Weak Coupling In the weak-coupling regime, the Markov approximation applies, and in Eq. (3.47) $C_\pm(t')$ can be replaced with $C_\pm(t)$, with the time integrals being ζ-functions. In particular, when the field is initially not excited, then the second term on the right-hand side of Eq. (3.47) vanishes and we are left with a homogeneous first-order differential equation, whose solution is, in analogy to Eq. (3.21),

$$C_\pm(t) = e^{(-\Gamma_\pm/2+i\delta_\pm)t}C_\pm(0), \tag{3.50}$$

where ($\Gamma\equiv\Gamma_{AA}$, $\delta\equiv\delta_{AA}$)

$$\Gamma_\pm = \Gamma \pm \Gamma_{AB}\,, \tag{3.51}$$

$$\delta_\pm = \delta \pm \delta_{AB}\,, \tag{3.52}$$

$$\Gamma_{AB} = \frac{2\omega_A^2}{\hbar\varepsilon_0 c^2}\,\mathbf{d}_A \mathrm{Im}\,\boldsymbol{G}(\mathbf{r}_A,\mathbf{r}_B,\omega_A)\mathbf{d}_B\,, \tag{3.53}$$

$$\delta_{AB} = \frac{\mathcal{P}}{\pi\hbar\varepsilon_0}\int_0^\infty \mathrm{d}\omega\,\frac{\omega^2}{c^2}\frac{\mathbf{d}_A\mathrm{Im}\,\boldsymbol{G}(\mathbf{r}_A,\mathbf{r}_B,\omega)\mathbf{d}_B}{\omega-\omega_A}\,. \tag{3.54}$$

Clearly, $\Gamma_\pm$ are the decay rates of the states $|\pm\rangle$, and the assumption (3.45) means that the two atoms are positioned in such a way that they have equal single-atom decay rates and line shifts. Note that the values of Γ_+ and Γ_- can substantially differ from each other, because of the interference term Γ_{AB} (of positive or negative sign).

Strong Coupling In the strong-coupling regime, the atoms are predominantly coupled (in a resonator-like equipment) to a sharp field resonance, whose mid-frequency approximately equals the atomic transition frequency. As a result, the atomic probability amplitudes in Eq. (3.47) must not necessarily be slowly varying compared with the kernel functions and the Markov approximation thus fails in general. Regarding the line shape of the field resonance as being a Lorentzian, one can of course approximate the kernels $K(t-t')$, $K_{AB}(t-t')$ [and

$K_{AD}(t-t')$ and $K_{BD}(t-t')$] in a similar way as done in Eq. (3.24) for a single atom.

Equation (3.47) reveals that the motion of the states $|\pm\rangle$ defined by Eq. (3.49) is governed by the kernel functions $K_{\pm}(t-t')$, and it may happen that one of them becomes very small, because of destructive interference [cf. Eq. (3.48)]. In that case, either $|+\rangle$ or $|-\rangle$ is weakly coupled to the field, and thus the strong-coupling regime cannot be realized for both of these states simultaneously.

4 BULK MEDIUM

The formalism outlined in Section 3 requires knowledge of the permittivity as a function of space and frequency. The spatial variation is typically determined by some arrangement of macroscopic bodies, each of which being characterized by a permittivity that is a function of frequency only. The frequency response of a dielectric body depends on its atomic structure and can be measured with high precision. For theoretical studies it may be useful to have some analytical expression at hand.

4.1 Drude–Lorentz Model

In the Drude–Lorentz model, which is widely used in practice, the permittivity is given by

$$\varepsilon(\omega) = 1 + \sum_{\alpha} \frac{\omega_{P\alpha}^2}{\omega_{T\alpha}^2 - \omega^2 - i\omega\gamma_\alpha}\,, \tag{4.1}$$

where $\omega_{T\alpha}$ and γ_α are the medium oscillation frequencies and linewidths, respectively, and $\omega_{P\alpha}$ correspond to the coupling constants. It is worth noting that the Drude–Lorentz model covers both dielectric ($\omega_{T\alpha}\neq 0$) and metallic ($\omega_{T\alpha}=0$) matter. An example of the permittivity for a (single-resonance) dielectric as a function of frequency is shown in Fig. 1. From the permittivity, the refractive index can be obtained according to the relations

$$n(\omega) = \sqrt{\varepsilon(\omega)} = n_R(\omega) + i n_I(\omega), \tag{4.2}$$

$$n_{R(I)}(\omega) = \sqrt{\frac{1}{2}\left[\sqrt{\varepsilon_R^2(\omega) + \varepsilon_I^2(\omega)} + (-)\,\varepsilon_R(\omega)\right]}. \tag{4.3}$$

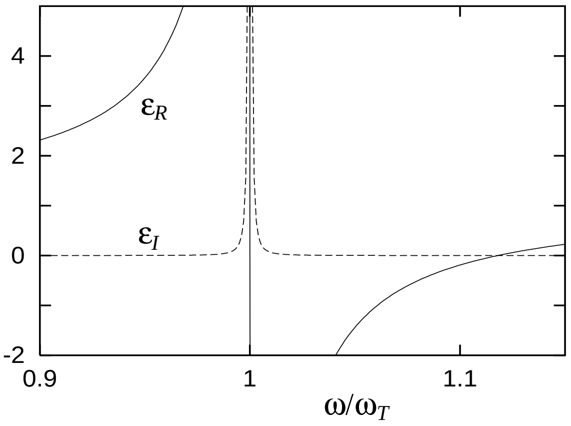

Figure 1: Real and imaginary parts of the permittivity of a single-resonance Drude–Lorentz-type dielectric for $\omega_P = 0.5\,\omega_T$ and $\gamma = 10^{-4}\,\omega_T$. The band gap covers the interval from ω_T to $\omega_L \simeq 1.12\,\omega_T$.

The Drude–Lorentz model features band gaps between the transverse frequencies $\omega_{T\alpha}$ and the longitudinal frequencies $\omega_{L\alpha} = \sqrt{\omega_{T\alpha}^2 + \omega_{P\alpha}^2}$. Far from a medium resonance, we typically observe that

$$\varepsilon_I(\omega) \ll |\varepsilon_R(\omega)|. \tag{4.4}$$

For $\omega < \omega_{T\alpha}$ (outside a band gap) we have

$$\varepsilon_R(\omega) > 1, \tag{4.5}$$

$$n_R(\omega) \simeq \sqrt{\varepsilon_R(\omega)} \gg n_I(\omega) \simeq \frac{\varepsilon_I(\omega)}{2\sqrt{\varepsilon_R(\omega)}}\,, \tag{4.6}$$

and for $\omega_{T\alpha} < \omega < \omega_{L\alpha}$ (inside a band gap)

$$\varepsilon_R(\omega) < 0, \tag{4.7}$$

$$n_R(\omega) \simeq \frac{\varepsilon_I(\omega)}{2\sqrt{|\varepsilon_R(\omega)|}} \ll n_I(\omega) \simeq \sqrt{|\varepsilon_R(\omega)|}\,. \tag{4.8}$$

When (inside a band gap)

$$\varepsilon_R(\omega) < -1 \tag{4.9}$$

is valid, which, in view of Eq. (4.1), leads to

$$\omega < \sqrt{\omega_{T\alpha}^2 + \tfrac{1}{2}\,\omega_{P\alpha}^2}\,, \tag{4.10}$$

then the Drude–Lorentz model also incorporates surface-guided waves [see, e.g., Raether (1988); Ho *et al.* (2001)], which are observed in the presence of an interface. These waves are bound to the interface, with the amplitudes being damped into either of the neighboring media. Typical examples are surface phonon polaritons for dielectrics and surface plasmon polaritons for metals. Note that in any case $\varepsilon_I(\omega) > 0$ is valid.

4.2 Local-Field Correction

From simple arguments based on the change of the mode density, it was suggested that the spontaneous emission rate of an atom inside a nonabsorbing medium should be modified according to $\Gamma = n\Gamma_0$, where n is the (real) refractive index of the medium and Γ_0 is given by Eq. (3.18) [Dexter (1956); di Bartolo (1968); Yariv (1975); Nienhuis *et al.* (1976)]. In this formula, it is assumed that the local field the atom interacts with is the medium-assisted electromagnetic field obtained by averaging over a region which contains a great number of medium constituents. In reality, the atom is located in a small region of free space, and the field therein differs from the averaged field. This effect is usually taken into consideration by introduction of a local-field correction factor ξ, thus

$$\Gamma = n\xi\Gamma_0 \,. \tag{4.11}$$

In the (Clausius–Mosotti) virtual-cavity model it is given by [Knoester *et al.* (1989); Milonni (1995)]

$$\xi = \left(\frac{n^2+2}{3}\right)^2 , \tag{4.12}$$

and in the (Onsager) real-cavity model by [Glauber *et al.* (1991)]

$$\xi = \left(\frac{3n^2}{2n^2+1}\right)^2 . \tag{4.13}$$

For absorbing media it was suggested that the index of refraction should be replaced by its real part and the square of the correction factor in Eqs. (4.12) and (4.13) by the absolute square [Barnett *et al.* (1992, 1996); Juzeliūnas (1997)]. Later it was found, on the basis of the quantization scheme outlined in Section 2, that a proper inclusion of the (quantum) noise polarization leads to a more complicated form of the local-field correction [Scheel *et al.* (1999a,b)], which (for the virtual-cavity model) was confirmed by an alternative, microscopic approach [Fleischhauer (1999)].

In contrast to the virtual cavity model where the modification of the field outside the cavity is disregarded, in the real-cavity model the mutual modification of the field outside and inside the cavity are taken into account in a consistent way. Experiments suggested that the real-cavity model is suitable for describing the decay of substitutional guest atoms different from the constituents of the medium [Rikken *et al.* (1995); de Vries *et al.* (1998); Schuurmans *et al.* (1998)].

Let us consider an excited atom placed at the center of an empty, spherical cavity (embedded in an otherwise homogeneous medium). According to Eq. (3.22) and the Green tensor given in Appendix A.2, the decay rate can be given in the form of [Scheel *et al.* (1999b)]

$$\Gamma = \Gamma_0 \left[1 + \mathrm{Re}\, C_1^N(\omega_A)\right] , \tag{4.14}$$

where the generalized reflection coefficient $C_1^N(\omega)$ reads [$\tilde{k} = \tilde{k}(\omega) = R\omega/c$]

$$\begin{aligned} C_1^N(\omega) = {} & e^{i\tilde{k}}\big\{i + \tilde{k}[n(\omega)+1] - i\tilde{k}^2 n(\omega) \\ & - \tilde{k}^3 n^2(\omega)/[n(\omega)+1]\big\}\big\{\sin\tilde{k} - \tilde{k}[\cos\tilde{k} \\ & + in(\omega)\sin\tilde{k}] + i\tilde{k}^2 n(\omega)\cos\tilde{k} - \tilde{k}^3[\cos\tilde{k} \\ & - in(\omega)\sin\tilde{k}]n^2(\omega)/[n^2(\omega)-1]\big\}^{-1}. \end{aligned} \tag{4.15}$$

As long as the surrounding medium can be treated as a continuum, Eq. (4.14) [together with Eq. (4.15)] is exact. It is valid for arbitrary cavity radius and arbitrary complex refractive index, without restriction to transition frequencies far from medium resonances.

When the cavity radius is much smaller than the wavelength of the atomic transition, i.e., $R\omega_A/c = \tilde{k}(\omega_A) \ll 1$, then the real-cavity model of local-field correction is realized. In this case, $C_1^N(\omega_A)$ can be expanded in powers of $\tilde{k}(\omega_A)$ to obtain [Scheel *et al.* (1999b); Tomaš (2001)]

$$\begin{aligned} \Gamma = \Gamma_0 & \left|\frac{3\varepsilon}{2\varepsilon+1}\right|^2 \Bigg\{ n_R \\ & + \frac{\varepsilon_I}{|\varepsilon|^2}\Bigg[\left(\frac{c}{\omega_A R}\right)^3 + \frac{28|\varepsilon|^2+16\varepsilon_R+1}{5|2\varepsilon+1|^2}\left(\frac{c}{\omega_A R}\right) \\ & - \frac{2}{|2\varepsilon+1|^2}\left(2n_I|\varepsilon|^2 + n_I\varepsilon_R + n_R\varepsilon_I\right)\Bigg]\Bigg\} \\ & + O(\omega_A R/c), \end{aligned} \tag{4.16}$$

where the dependence of the permittivity ε and the refractive index n on ω_A has been suppressed. For $\varepsilon_I(\omega_A) = 0$, i.e, when material absorption is fully disregarded, Eq. (4.16) reproduces exactly local-field correction factor (4.13). The second term in the curly brackets essentially results from absorption. It is seen that material absorption gives rise to a strong dependence of the decay rate on the cavity radius. In particular, the leading term proportional to R^{-3} can

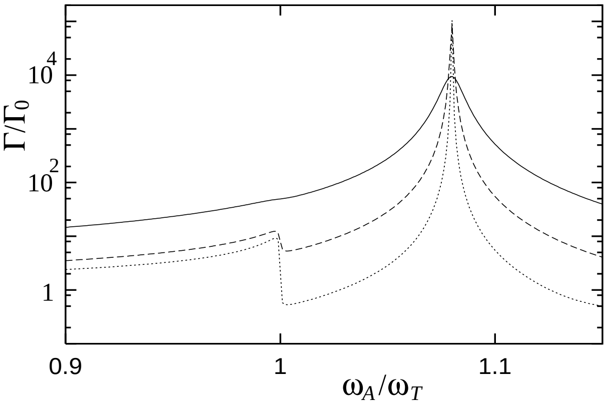

Figure 2: Spontaneous decay rate [Eq. (4.14)] of an atom embedded in a dielectric medium as a function of the atomic transition frequency near a medium resonance for a single-resonance Drude–Lorentz-type dielectric [$\omega_{\mathrm{P}} = 0.5\,\omega_T$; $\gamma/\omega_T = 10^{-2}$ (solid line), 10^{-3} (dashed line), and 10^{-4} (dotted line)]. The (real-) cavity radius is $R = 0.02\,\lambda_T$.

be regarded as corresponding to nonradiative energy transfer from the atom to the medium. Examples of the dependence of rate of spontaneous decay on the atomic transition frequency are plotted in Fig. 2 for a Drude–Lorentz-type dielectric medium. It is seen that in the band-gap region (where for a non-absorbing medium spontaneous emission would be inhibited) the decay rate can drastically increase, because of the non-radiative decay channel associated with absorption. Note that the strongest enhancement of spontaneous decay is observed at $\omega_A \simeq \sqrt{\omega_T^2 + \frac{3}{2}\omega_P^2}$, which [for small values of $\varepsilon_I(\omega_A)$] corresponds to $2\varepsilon(\omega_A) + 1 \simeq 0$.

5 PLANAR SURFACE

Let us turn to the problem of spontaneous decay of an excited atom located near the surface of a half-space medium. For real permittivity, configurations of that type have been studied extensively in connection with Casimir and van der Waals forces [see, e.g., Meschede *et al.* (1990); Fichet *et al.* (1995) and references therein] and with regard to scanning near-field optical microscopy [see, e.g., Henkel *et al.* (1998)].

To be more specific, let us consider two infinite half-spaces such that

$$\varepsilon(\mathbf{r},\omega) = \begin{cases} \varepsilon(\omega) & \text{if} \quad z \le 0 \\ 1 & \text{if} \quad z > 0 \end{cases} . \tag{5.1}$$

For $z > 0$, the reflection part of the Green tensor reads [Maradudin *et al.* (1975); Mills *et al.* (1975); Tomaš (1995); Ho *et al.* (1998)]

$$G^R_{xx}(z,z,\omega) = -\frac{i}{8\pi k^2}\int_0^\infty \mathrm{d}k_\parallel\, k_\parallel \beta\, \mathrm{e}^{2i\beta z} r^p(k_\parallel) + \frac{i}{8\pi}\int_0^\infty \mathrm{d}k_\parallel\, \frac{k_\parallel \mathrm{e}^{2i\beta z}}{\beta}\, r^s(k_\parallel), \tag{5.2}$$

$$G^R_{yy}(z,z,\omega) = G^R_{xx}(z,z,\omega), \tag{5.3}$$

$$G^R_{zz}(z,z,\omega) = \frac{i}{4\pi k^2}\int_0^\infty \mathrm{d}k_\parallel\, k_\parallel^3 \frac{\mathrm{e}^{2i\beta z}}{\beta}\, r^p(k_\parallel) \tag{5.4}$$

[$k = \omega/c$, $\beta = (k^2 - k_\parallel^2)^{1/2}$], where $r^p(k_\parallel)$ and $r^s(k_\parallel)$ are respectively the familiar Fresnel reflection coefficients for *p*- (TM) and *s*- (TE) polarized waves. Substitution of these expressions ($\omega = \omega_A$) into Eqs. (3.22) and (3.23) yields the decay rate and the line shift of an atom at a distance *z* from the surface [Agarwal (1975); Agarwal *et al.* (1977); Scheel *et al.* (1999c)], which are in agreement with classical results [see, e.g., Chance *et al.* (1978) and references therein].

When the distance of the atom from the surface is small compared to the wavelength, $kz \ll 1$, then the integrals in Eqs. (5.2) – (5.4) can be evaluated asymptotically to give [Scheel *et al.* (1999c)]

$$G^R_{zz}(z,z,\omega) = \frac{1}{16\pi k^2 z^3}\,\frac{n^2(\omega)-1}{n^2(\omega)+1} + \frac{1}{8\pi z}\,\frac{[n(\omega)-1]^2}{n(\omega)[n(\omega)+1]} + \frac{ik}{12\pi}\,\frac{[n(\omega)-1][2n(\omega)-1]}{n(\omega)[n(\omega)+1]} + O(kz), \tag{5.5}$$

$$G^R_{xx}(z,z,\omega) = \tfrac{1}{2}G^R_{zz}(z,z,\omega) - \frac{1}{16\pi z}\,\frac{n^2(\omega)-1}{n^2(\omega)+1} - \frac{ik}{3\pi}\,\frac{n(\omega)-1}{n(\omega)+1} + O(kz), \tag{5.6}$$

$$G^R_{yy}(z,z,\omega) = G^R_{xx}(z,z,\omega). \tag{5.7}$$

Inserting Eqs. (5.5) – (5.7) into Eq. (3.22) yields

$$\Gamma = \frac{3\Gamma_0}{8}\left(1 + \frac{d_z^2}{d^2}\right)\left(\frac{c}{\omega_A z}\right)^3 \times \frac{\varepsilon_I(\omega_A)}{|\varepsilon(\omega_A)+1|^2} + O\!\left(\frac{c}{\omega_A z}\right). \tag{5.8}$$

The leading ($\sim z^{-3}$) term is the same as in the microscopic approach by Yeung *et al.* (1996). This term, which is proportional to $\varepsilon_I(\omega_A)$, is closely related to nonradiative decay, i.e., energy transfer from the atom to the medium. Obviously, a change of $\varepsilon_I(\omega_A)$ mostly affects the near-surface behavior of the decay rate. Note that the distance of the atom from the surface must not be smaller than interatomic distances in the medium (otherwise an interface cannot be defined). Examples of the spontaneous decay rate are shown in Fig. 3 for dielectric matter of Drude–Lorentz type. Note the strong absorption-assisted enhancement of spontaneous decay that is observed inside the band gap at $\omega_A \simeq \sqrt{\omega_T^2 + \frac{1}{2}\omega_P^2}$. It corresponds [for small values of $\varepsilon_I(\omega_A)$] to the condition $\varepsilon(\omega_A) + 1 \simeq 0$, which marks the position of the highest density of the surface-guided waves [cf. Eq. (4.10)].

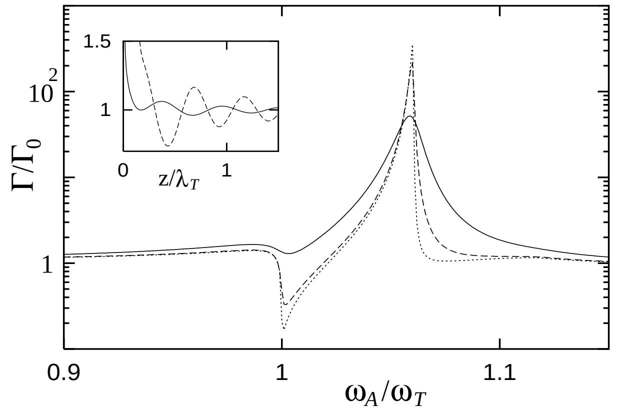

Figure 3: The rate of spontaneous decay of an excited atom near a planar dielectric half-space is shown as a function of the transition frequency for an x-oriented transition dipole moment and a single-resonance Drude–Lorentz-type dielectric [$\omega_\mathrm{P} = 0.5\,\omega_T$; $\gamma/\omega_T = 10^{-2}$ (solid line), 10^{-3} (dashed line), and 10^{-4} (dotted line); $z = 0.05\,\lambda_T$]. The inset illustrates the dependence on the distance of the decay rate [$\gamma/\omega_T = 10^{-3}$; $\omega_A/\omega_T = 0.9$ (solid line), 1.06 (dashed line)].

Similarly, from Eq. (3.23) together with Eqs. (5.5) – (5.7), the line shift due to the presence of the macroscopic body reads

$$\delta\omega_A = \frac{3\Gamma_0}{32}\left(1 + \frac{d_z^2}{d^2}\right)\left(\frac{c}{\omega_A z}\right)^3 \times \frac{|\varepsilon(\omega_A)|^2 - 1}{|\varepsilon(\omega_A) + 1|^2} + O\!\left(\frac{c}{\omega_A z}\right). \qquad (5.9)$$

In contrast to the decay rate, here the leading ($\sim z^{-3}$) term even appears when absorption is disregarded [$\varepsilon_I(\omega_A) = 0$].

6 SPHERICAL MICRORESONATOR

In Section 4.2, an atom in a microsphere whose radius is much smaller than the wavelength of the atomic transition was considered. If the radius is not small compared with the wavelength, the cavity can act as a resonator. It is well known that the spontaneous decay of an excited atom can be strongly modified when it is placed in a microresonator [Hinds (1991); Haroche (1992); Meschede (1992); Meystre (1992); Berman (Ed., 1994); Kimble (1998)]. There are typically two qualitatively different regimes: the weak-coupling regime and the strong-coupling regime. In the weak-coupling regime the Markov approximation applies and a monotonous exponential decay is observed, the decay rate being enhanced or reduced compared to the free-space value depending on whether the atomic transition frequency fits a cavity resonance or not. The strong-coupling regime, in contrast, is characterized by reversible Rabi oscillations where the energy of the initially excited atom is periodically exchanged between the atom and the radiation field. This usually requires that the emission is in resonance with a high-quality cavity mode.

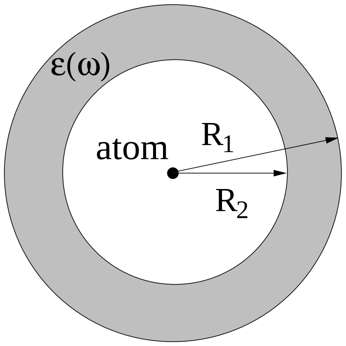

Figure 4: Scheme of the spherical microresonator.

Let us consider an excited atom placed at the center of a spherical three-layer structure (Fig. 4). The outer layer ($r > R_1$) and the inner layer ($0 \le r < R_2$) are vacuum, whereas the middle layer ($R_2 \le r \le R_1$), which plays the role of the resonator wall, is matter. In particular for a Drude–Lorentz-type dielectric, the wall would be perfectly reflecting in the band-gap zone, provided that absorption could be disregarded. Restricting our attention to a true resonator, we may assume that the condition $R_2\omega_A/c \gg 1$ is satisfied.

6.1 Weak Coupling

From Eq. (1.3) together with the Green tensor for a spherical three-layer structure as given in Appendix A.2, the decay rate becomes [Ho *et al.* (2000)]

$$\begin{aligned}\Gamma &\simeq \Gamma_0\,\mathrm{Re}\left[\frac{n(\omega_A) - i\tan(\omega_A R_2/c)}{1 - i n(\omega_A)\tan(\omega_A R_2/c)}\right] \\ &= \Gamma_0\, n_R(\omega_A)[1+\tan^2(\omega_A R_2/c)] \\ &\quad \times \Big\{[1+n_I(\omega_A)\tan(\omega_A R_2/c)]^2 \\ &\qquad + n_R^2(\omega_A)\tan^2(\omega_A R_2/c)\Big\}^{-1}. \qquad (6.1)\end{aligned}$$

Note that in Eq. (6.1) it is assumed that $\exp[-i n_I(\omega_A)(R_1-R_2)\omega_A/c] \ll 1$ (thick cavity wall).

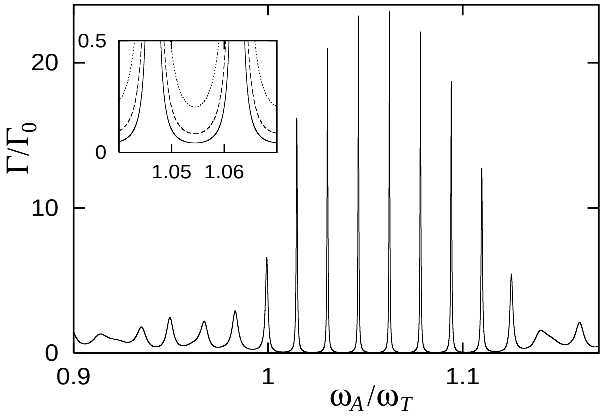

Figure 5: The rate of spontaneous decay of an excited atom at the center of a spherical microresonator is shown as a function of the transition frequency for a single-resonance Drude–Lorentz-type dielectric wall ($R_2 = 30\,\lambda_T$; $R_1 - R_2 = \lambda_T$; $\omega_\mathrm{P} = 0.5\,\omega_T$; $\gamma = 10^{-2}\omega_T$). The curves in the inset correspond to $\gamma/\omega_T = 10^{-2}$ (solid line), 2×10^{-2} (dashed line), and 5×10^{-2} (dotted line). [After Ho *et al.* (2000).]

The dependence on the transition frequency of the decay rate is illustrated in Fig. 5. It is seen that the decay rate very sensitively depends on the transition frequency. Narrow-band enhancement of spontaneous decay ($\Gamma/\Gamma_0 > 1$) alternates with broadband inhibition ($\Gamma/\Gamma_0 < 1$). The frequencies at which the maxima of enhancement are observed correspond to the resonance frequencies of the cavity. Within the band gap the heights and widths of the frequency intervals in which spontaneous decay is feasible are essentially determined by material absorption. Outside the band-gap zone the change of the decay rate is less pronounced, because of the relatively large input-output coupling, the (small) material absorption being of secondary importance.

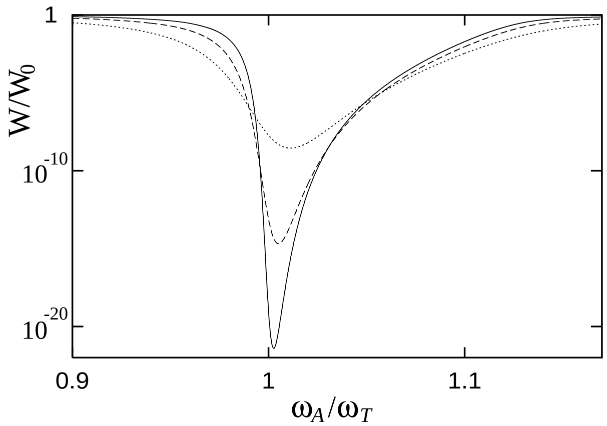

Figure 6: The amount of the (outside the resonator) available radiation energy after spontaneous decay of an excited atom at the center of a spherical microresonator is shown as a function of the transition frequency for a single-resonance Drude–Lorentz-type dielectric wall [$\gamma/\omega_T = 10^{-2}$ (solid line), 2×10^{-2} (dashed line), 5×10^{-2} (dotted line); the other parameters are the same as in Fig. 5]. [After Ho *et al.* (2000).]

The widths of the resonance lines are responsible for the damping of the corresponding intracavity field (mode). There are two damping mechanisms: photon leakage to the outside of the cavity and photon absorption by the cavity-wall material. The first mechanism is the dominant one outside bands in regions where normal dispersion ($\mathrm{d}n_R/\mathrm{d}\omega > 0$) is observed, while the latter dominates inside band gaps where anomalous dispersion ($\mathrm{d}n_R/\mathrm{d}\omega < 0$) is observed. To illustrate this in more detail, let us consider the total amount of radiation energy observed outside the cavity and compare it with the energy $W_0 = \hbar\omega_\mathrm{A}$ emitted by an atom in free space. Application of Eq. (3.37) [together with Eqs. (3.34) and (3.36)] yields [Ho *et al.* (2000)]

$$\frac{W}{W_0} \simeq \frac{|\mathcal{A}_l^N(\omega_\mathrm{A})|^2}{1+\mathrm{Re}\,\mathcal{C}_l^N(\omega_\mathrm{A})}\,, \tag{6.2}$$

with $\mathcal{A}_l^N(\omega_\mathrm{A})$ and $\mathcal{C}_l^N(\omega_\mathrm{A})$ being given according to Eqs. (A.34) and (A.35) respectively. Examples of the dependence of W/W_0 on the atomic transition frequency are plotted in Fig. 6. It is seen that inside the band gap most of the energy emitted by the atom is absorbed by the cavity wall in the course of time, while outside the band gap the absorption is (for the chosen values of γ) much less significant. Note that with increasing value of γ the band gap is smoothed a little bit, and thus the fraction of light that escapes from the cavity can increase.

6.2 Strong Coupling

When the coupling between the atom and a cavity resonance (mid-frequency ω_C, line width $\Delta\omega_C$) is so strong that the (weak-coupling) decay rate becomes comparable to the cavity line width, $\Gamma_C \gtrsim \Delta\omega_C$, the Markov approximation is no longer adequate. In this case, the integral equation (3.13) or approximate equations of the type (3.25) and (3.26) should be used in order to describe the temporal evolution of the (upper) atomic state. For the configuration under investigation, the cavity line width can be given by

$$\Delta\omega_C = \frac{c\Gamma_0}{R_2\Gamma_C}\,. \tag{6.3}$$

Inside a band gap, Γ_C is essentially determined by material absorption. In particular, the single-resonance Drude–Lorentz model reveals that

$$\begin{aligned}\Gamma_C &\simeq \Gamma_0\,\frac{n_I^2(\omega_C)+1}{n_R(\omega_C)}\\ &\simeq \Gamma_0\,\frac{2\sqrt{(\omega_L^2-\omega_C^2)(\omega_C^2-\omega_T^2)}}{\gamma\omega_C}\end{aligned} \tag{6.4}$$

($\gamma \ll \omega_T, \omega_P, \omega_P^2/\omega_T$). Below the band gap radiative losses dominate and Γ_C reads

$$\Gamma_C \simeq \Gamma_0\, n_R(\omega_C) \simeq \Gamma_0\sqrt{\frac{\omega_L^2-\omega_C^2}{\omega_T^2-\omega_C^2}} \tag{6.5}$$

($n_R \gg n_I$).

Typical examples of the time evolution of the upper-state occupation probability are shown in Fig. 7. The curves are the exact (numerical) solutions of the integral equation (3.13) [together with the kernel function (3.17)] for a (single-resonance) dielectric wall of Drude–Lorentz type. The figure shows that with increasing value of the intrinsic absorption constant γ of the wall material the Rabi oscillations become less pronounced. Clearly, larger values of γ mean enlarged absorption probability of the emitted photon by the cavity wall and thus reduced probability of atom-field energy interchange.

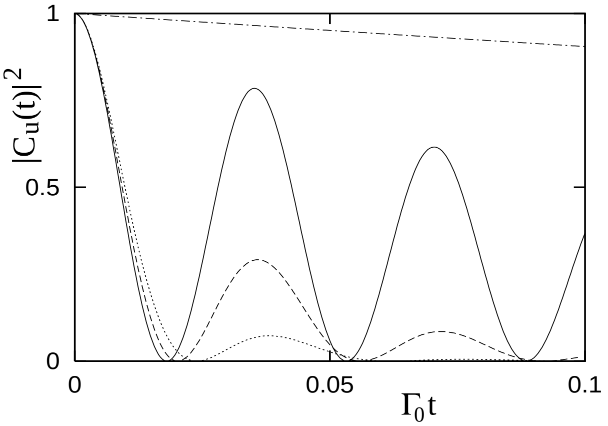

Figure 7: The temporal evolution of the occupation probability of the upper state of an initially excited atom at the center of a spherical microresonator is shown for a single-resonance Drude–Lorentz-type dielectric wall [$R_2 = 30\,\lambda_T$; $R_1 - R_2 = \lambda_T$; $\omega_\mathrm{P} = 0.5\,\omega_T$; $\omega_A = 1.046448\,\omega_T$; $\Gamma_0\lambda_T/(2c) = 10^{-6}$; $\gamma/\omega_T = 10^{-4}$ (solid line), 5×10^{-4} (dashed line), 10^{-3} (dotted line)]. For comparison, the exponential decay in free space is shown (dashed-dotted line). [After Ho *et al.* (2000).]

7 MICROSPHERE

Light propagating in a dielectric sphere can be trapped by repeated total internal reflections. When the round-trip optical path fits integer numbers of the wavelength, whispering gallery (WG) waves are formed, which combine extreme photonic confinement with very high quality factors [Collot *et al.* (1993); Chang *et al.* (1996); Gorodetsky *et al.* (1996); Vernooy *et al.* (1998); Uetake *et al.* (1999)] – properties that are crucial for cavity QED experiments [Lin *et al.* (1992); Barnes *et al.* (1996); Lermer *et al.* (1998); Vernooy *et al.* (1998); Fujiwara *et al.* (1999); Yukawa *et al.* (1999)] and certain optoelectronical applications [Chang *et al.* (1996)]. WG waves are commonly classified by means of three numbers [Collot *et al.* (1993); Chang *et al.* (1996)]: the angular-momentum number l, the azimuthal number m, and the number i of radial maxima of the field inside the sphere. In the case of a uniform sphere, the WG waves are $(2l+1)$-fold degenerate, i.e., the $2l+1$ azimuthal resonances belong to the same frequency $\omega_{l,i}$.

A dielectric microsphere whose permittivity is of Drude–Lorentz type does not only give rise to WG waves, but can also feature surface-guided (SG) waves inside band-gap regions.[2] In contrast to WG waves, each angular-momentum number l is associated with only one SG wave.

If an excited atom is situated near a dielectric microsphere, spontaneous decay sensitively depends on whether or not the transition is tuned to a WG or an SG resonance. Moreover, whereas WG waves typically suffer from material absorption, the effect of material absorption on SG waves is weak in general.

7.1 Decay Rate

Applying Eq. (3.22) together with the Green tensor of a microsphere (Appendix A.2), the spontaneous decay rate for a (with respect to the sphere) radially oriented dipole moment can be given by

$$\Gamma^{\perp} = \Gamma_0 \Bigg\{ 1 + \tfrac{3}{2} \sum_{l=1}^{\infty} \Bigg[l(l+1)(2l+1) \times \mathrm{Re}\Bigg(\mathcal{B}_l^N(\omega_A) \bigg[\frac{h_l^{(1)}(k_A r_A)}{k_A r_A} \bigg]^2 \Bigg) \Bigg] \Bigg\}, \tag{7.1}$$

and for a tangential dipole it reads

$$\Gamma^{\parallel} = \Gamma_0 \Bigg\{ 1 + \tfrac{3}{4} \sum_{l=1}^{\infty} \Bigg[(2l+1) \times \mathrm{Re}\Bigg(\mathcal{B}_l^M(\omega_A) \Big[h_l^{(1)}(k_A r_A) \Big]^2 + \mathcal{B}_l^N(\omega_A) \bigg[\frac{\big[k_A r_A h_l^{(1)}(k_A r_A)\big]'}{k_A r_A} \bigg]^2 \Bigg) \Bigg] \Bigg\} \tag{7.2}$$

($k_A = \omega_A/c$), where $\mathcal{B}_l^N(\omega_A)$ is defined according to Eq. (A.30), and the prime indicates the derivative with respect to $k_A r_A$ [Ho *et al.* (2001)].[3] Note that a radially oriented transition dipole moment only couples to TM waves, whereas a tangentially oriented dipole moment couples to both TM and TE waves.

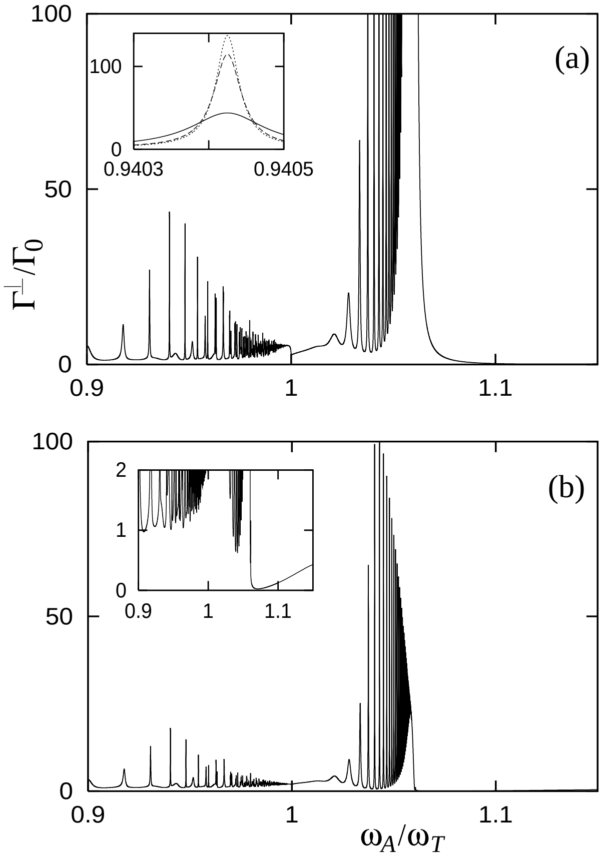

Figure 8: The rate of spontaneous decay of an excited atom near a microsphere is shown as a function of the transition frequency for a radially oriented transition dipole moment and a single-resonance Drude–Lorentz-type dielectric [$R=2\,\lambda_T$; $\omega_P=0.5\,\omega_T$; $\gamma/\omega_T=10^{-4}$; (a) $\Delta r=0.02\,\lambda_T$; inset: $\gamma/\omega_T=10^{-4}$ (solid line), 10^{-5} (dashed line), 10^{-6} (dotted line); (b) $\Delta r=0.1\,\lambda_T$]. [After Ho *et al.* (2001).]

It is worth noting that when the atom is very close to the microsphere, then the decay rates Eqs. (7.1) and (7.2) reduce to exactly the same form as in Eq. (5.8) for a planar interface, with z being now the distance between the atom and the surface of the microsphere. Obviously, nonradiative decay, which dominates in this case, does not respond sensitively to the actual radiation-field structure.

The dependence on the transition frequency of the decay rate, as it is typically observed for not too small (large) values of the atom-surface distance (material absorption), is illustrated in Fig. 8 for a radially oriented transition dipole moment. Since it mimics the single-quantum excitation spectrum of the sphere-assisted (TM) radiation field, the figure reveals that both the WG and SG field resonances can strongly enhance the spontaneous decay. Material absorption broadens the resonance lines at the expense of the heights, and the enhancement is accordingly reduced [see the inset in Fig. 8(a)]. Clearly, the sphere-assisted enhancement of spontaneous decay decreases with increasing distance between the atom and the sphere [compare Figs. 8(a) and (b)].

---

[2] For the dependence on frequency of the quality factors of WG and SG waves, see Ho *et al.* (2001).

[3] Equations (7.1) and (7.2) can be regarded as being the natural extension of the (classical) theory for nonabsorbing matter as given by Chew(1987) and Klimov *et al.* (1996). Note that when the formulas for nonabsorbing matter are given in terms of the Green tensor, without an explicit decomposition in real and imaginary parts, then for the real permittivity the complex one can be substituted.

Figure 8 also reveals that SG waves can give rise to a much stronger enhancement of the spontaneous decay than WG waves. In particular, with increasing angular-momentum number the SG field resonance lines strongly overlap and huge enhancement [e.g., of the order of magnitude of 10^4 for the parameters chosen in Fig. 8(a)] can be observed for transition frequencies inside a band gap. When the distance between the atom and the sphere increases, then the atom rapidly decouples from that part of the field. Thus, the huge enhancement of spontaneous decay rapidly reduces and the interval in which inhibition of spontaneous decay is typically observed, extends accordingly [see Fig. 8(b)].

7.2 Frequency Shift

The sphere-assisted frequency shift calculated from Eq. (3.23) together with the Green tensor given in Appendix A.2 reads

$$\delta\omega_A^{\perp} = -\frac{3\Gamma_0}{4}\sum_{l=1}^{\infty}\Bigg[l(l+1)(2l+1) \times \mathrm{Im}\bigg(\mathcal{B}_l^N(\omega_A)\left[\frac{h_l^{(1)}(k_A r_A)}{k_A r_A}\right]^2\bigg)\Bigg] \tag{7.3}$$

for a radially oriented transition dipole moment, and

$$\delta\omega_A^{\parallel} = -\frac{3\Gamma_0}{8}\sum_{l=1}^{\infty}\Bigg[(2l+1) \times \mathrm{Im}\bigg(\mathcal{B}_l^M(\omega_A)\left[h_l^{(1)}(k_A r_A)\right]^2 + \mathcal{B}_l^N(\omega_A)\left[\frac{\left[k_A r_A h_l^{(1)}(k_A r_A)\right]'}{k_A r_A}\right]^2\bigg)\Bigg] \tag{7.4}$$

for a tangentially oscillating dipole.[4] Note that the small quantum corrections that arise from the second term in Eq. (3.23) have been omitted. For very small distance between the atom and the sphere, Eqs. (7.3) and (7.4) acquire the same form as for a planar interface, Eq. (5.9).

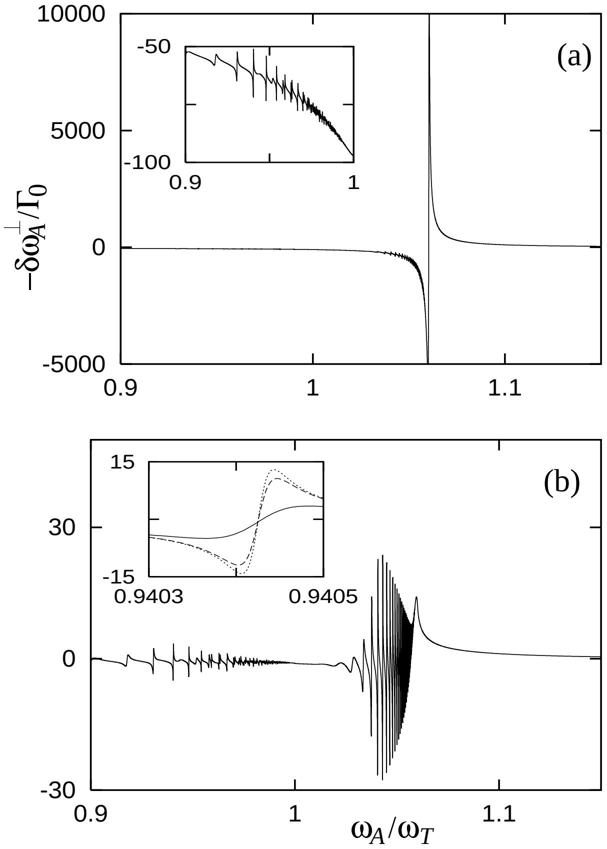

Figure 9: The frequency shift in spontaneous decay of an excited atom near a microsphere is shown as a function of the transition frequency for a radially oriented transition dipole moment and a single-resonance Drude–Lorentz-type dielectric [$R = 2\,\lambda_T$; $\omega_P = 0.5\,\omega_T$; $\gamma/\omega_T = 10^{-4}$; (a) $\Delta r = 0.02\,\lambda_T$; (b)$\Delta r = 0.1\,\lambda_T$; inset: $\gamma/\omega_T = 10^{-4}$ (solid line), 10^{-5} (dashed line), 10^{-6} (dotted line)]. [After Ho *et al.* (2001).]

In Fig. 9, an example of the dependence on the transition frequency of the frequency shift for a radially oriented dipole is shown. It is seen that the field resonances can give rise to noticeable frequency shifts in the very vicinities of the corresponding resonance frequencies. Transition frequencies that are lower (higher) than a resonance frequency are shifted to lower (higher) frequencies. In close analogy to the behavior of the decay rate, the frequency shift is more pronounced for SG resonances than for WG resonances and can be huge for large angular-momentum numbers when the lines of the SG field resonances strongly overlap.

---

[4] Again, Eqs. (7.3) and (7.4) could be obtained from the classical theory for nonabsorbing matter [Klimov *et al.* (1996)]; see footnote 3 on page 16.

The behavior of the frequency shift as shown in Fig. 9(b) can already be seen in the single-resonance approximation [Ching *et al.* (1987)]. Let the atomic transition frequency ω_A be close to a resonance frequency ω_C of the microsphere and assume that, in a first approximation, the effect from the other resonances may be ignored. For a Lorentzian resonance line of width $\Delta\omega_C$, from Eq. (1.4) it then follows that

$$\begin{aligned}\delta\omega_A &\simeq -\frac{\mathcal{P}}{4\pi}\int_{-\infty}^{\infty}\mathrm{d}\omega\,\frac{1}{\omega-\omega_A}\,\frac{\Gamma_C\Delta\omega_C^2}{(\omega-\omega_C)^2+\Delta\omega_C^2}\\ &= -\frac{\Gamma_C\Delta\omega_C}{2}\,\frac{\omega_A-\omega_C}{(\omega_A-\omega_C)^2+\Delta\omega_C^2}\,, \end{aligned}\qquad(7.5)$$

where Γ_C (which corresponds to the height of the line) is the decay rate for $\omega_A=\omega_C$. In particular, Eq. (7.5) indicates that the frequency shift peaks at half maximum on both sides of the resonance line. With increasing material absorption, the linewidth $\Delta\omega_C$ increases while Γ_C decreases, and thus the absolute value of the frequency shift is reduced, the distance between the maximum and the minimum being somewhat increased. With decreasing distance between the atom and the microsphere near-field effects become important and Eq. (7.5) fails, as it can be seen from a comparison of Figs. 9(a) and (b).

7.3 Emitted-Light Intensity

7.3.1 Spatial distribution

Substitution into Eq. (3.35) of the expression for the Green tensor (Appendix A.2) yields ($\theta_A=\phi_A=0$, $r_A\le r$)

$$\begin{aligned}\mathbf{F}^{\perp}(\mathbf{r},\mathbf{r}_A,\omega_A) &= \frac{k_A^3 d}{4\pi\varepsilon_0}\sum_{l=1}^{\infty}\Bigg\{(2l+1)\\ &\times\frac{1}{k_A r_A}\Big[j_l(k_A r_A)+\mathcal{B}_l^N(\omega_A)h_l^{(1)}(k_A r_A)\Big]\\ &\times\Bigg[\mathbf{e}_r\,l(l+1)\,\frac{h_l^{(1)}(k_A r)}{k_A r}\,P_l(\cos\theta)\\ &-\mathbf{e}_\theta\,\frac{[k_A r\,h_l^{(1)}(k_A r)]'}{k_A r}\,\sin\theta P_l'(\cos\theta)\Bigg]\Bigg\}\end{aligned}\qquad(7.6)$$

for a radially oriented transition dipole moment, and

$$\begin{aligned}\mathbf{F}^{\|}(\mathbf{r},\mathbf{r}_A,\omega_A) &= \frac{k_A^3 d}{4\pi\varepsilon_0}\sum_{l=1}^{\infty}\Bigg\{\frac{(2l+1)}{l(l+1)}\Bigg[\mathbf{e}_r\cos\phi\\ &\times\tilde{\mathcal{B}}_l^N l(l+1)\,\frac{h_l^{(1)}(k_A r)}{k_A r}\,\sin\theta P_l'(\cos\theta)\\ &+\mathbf{e}_\theta\cos\phi\Bigg(\tilde{\mathcal{B}}_l^M h_l^{(1)}(k_A r)P_l'(\cos\theta)\\ &+\tilde{\mathcal{B}}_l^N\,\frac{[k_A r\,h_l^{(1)}(k_A r)]'}{k_A r}\,\tilde{P}_l(\cos\theta)\Bigg)\\ &-\mathbf{e}_\phi\sin\phi\Bigg(\tilde{\mathcal{B}}_l^M h_l^{(1)}(k_A r)\tilde{P}_l(\cos\theta)\\ &+\tilde{\mathcal{B}}_l^N\,\frac{[k_A r\,h_l^{(1)}(k_A r)]'}{k_A r}\,P_l'(\cos\theta)\Bigg)\Bigg]\Bigg\}\end{aligned}\qquad(7.7)$$

for a tangentially oriented dipole in the xz-plane. Here the abbreviating notations

$$\begin{aligned}\tilde{\mathcal{B}}_l^N &= \frac{1}{k_A r_A}\Big\{[k_A r_A j_l(k_A r_A)]'\\ &+\mathcal{B}_l^N(\omega_A)[k_A r_A h_l^{(1)}(k_A r_A)]'\Big\},\end{aligned}\qquad(7.8)$$

$$\tilde{\mathcal{B}}_l^M = j_l(k_A r_A)+\mathcal{B}_l^M(\omega_A)h_l^{(1)}(k_A r_A),\qquad(7.9)$$

$$\tilde{P}_l(\cos\theta) = l(l+1)P_l(\cos\theta)-\cos\theta P_l'(\cos\theta)\qquad(7.10)$$

have been introduced. $|\mathbf{F}^{\perp(\|)}(\mathbf{r},\mathbf{r}_A,\omega_A)|^2$ determines, according to Eq. (3.34), the spatial distribution of the light emitted by a radially (tangentially) oriented dipole.

Let us restrict our attention to a radially oriented transition dipole moment. Examples of $|\mathbf{F}^{\perp}(\mathbf{r},\mathbf{r}_A,\omega_A)|^2$ are plotted in Fig. 10. In this case, the far field is essentially determined by $F_\theta^{\perp}$, as an inspection of Eq. (7.6) reveals. When the atomic transition frequency coincides with the frequency of a WG wave of angular-momentum number l far from the band gap [Fig. 10(a)], then the corresponding l-term in the series (7.6) obviously yields the leading contribution to the emitted radiation, whose angular distribution is significantly determined by the term $\sim\sin\theta\,P_l'(\cos\theta)$. Thus, the emission pattern has l lobes in, say, the yz-plane, i.e., l cone-shaped peaks around the z-axis, because of symmetry reasons. The lobes near $\theta=0$ and $\theta=\pi$ are the most dominant ones in general, because of

$$-\sin\theta P_l'(\cos\theta)\sim(\sin\theta)^{-1/2}+O\big(l^{-1}\big)\qquad(7.11)$$

($0<\theta\le\pi$). Note that the superposition of the leading term with the remaining terms in series (7.6) gives rise to some asymmetry with respect to the plane $\theta=\pi/2$.

When the atomic transition frequency approaches (from below) a band gap (but is still outside it), a

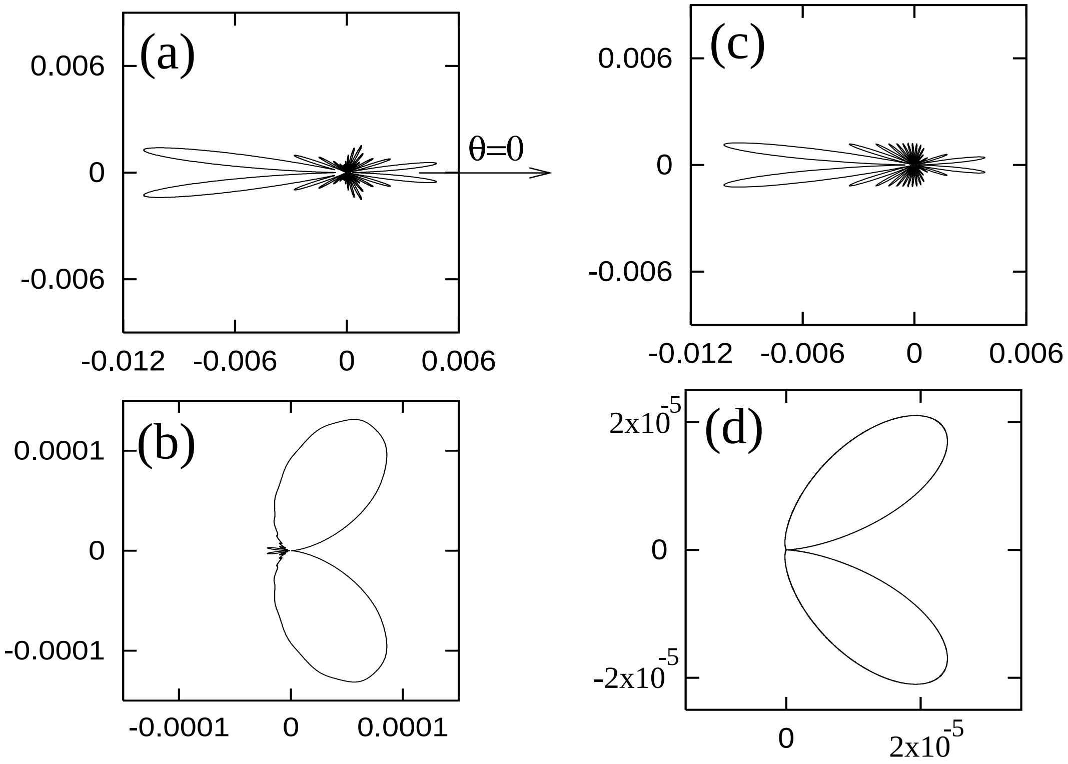

Figure 10: Polar diagrams of the far-field emission pattern $|\mathbf{F}^{\perp}(\mathbf{r},\mathbf{r}_A,\omega_A)|^2/(k_A^3 d/4\pi\varepsilon_0)^2$ of a radially oscillating dipole near a single-resonance Drude–Lorentz-type dielectric microsphere [$R = 2\,\lambda_T$; $\omega_P = 0.5\,\omega_T$; $\gamma/\omega_T = 10^{-4}$; $\Delta r = 0.02\,\lambda_T$; $r = 20\,\lambda_T$; $\omega_A/\omega_T = 0.94042$ (a), 0.999 (b), 1.02811 (c), 1.06 (d). [After Ho *et al.* (2001).]

strikingly different behavior is observed [Fig. 10(b)]. The emission pattern changes to a two-lobe structure similar to that observed in free space, but bent away from the microsphere surface, the emission intensity being very small. Since near a band gap absorption losses dominate, a photon that is resonantly emitted is almost certainly absorbed and does not contribute to the far field in general. If the photon is emitted in a lower-order WG wave where radiative losses dominate, it has a bigger chance to escape. The superposition of all these weak (off-resonant) contributions just form the two-lobe emission pattern observed, as it can also be seen from careful inspection of the series (7.6).

When the atomic transition frequency is inside a band gap and coincides with the frequency of a SG wave of low order such that the radiative losses dominate, then the emission pattern resembles that observed for resonant interaction with a low-order WG wave [compare Figs. 10(a) and (c)]. With increasing transition frequency the absorption losses become substantial and eventually change the emission pattern in a quite similar way as do below the band gap [compare Figs. 10(b) and (d)]. Obviously, the respective explanations are similar in the two cases.

7.3.2 Radiative versus nonradiative decay

Since the imaginary part of both the vacuum Green tensor $\boldsymbol{G}^V$ and the scattering term $\boldsymbol{G}^R$ is transverse, the decay rate (1.3) results from the coupling of the atom to the transverse part of the electromagnetic field. Nevertheless, the decay of the excited atomic state must not necessarily be accompanied by the emission of a real photon, but instead a matter quantum can be created, because of material absorption. To compare the two decay channels, let us consider, according to Eq. (3.37), the fraction W/W_0 of the atomic (transition) energy that is irradiated by an atom with a radially oriented transition dipole moment. Using Eqs. (3.34) and (7.6), one derives [Ho *et al.* (2001)]

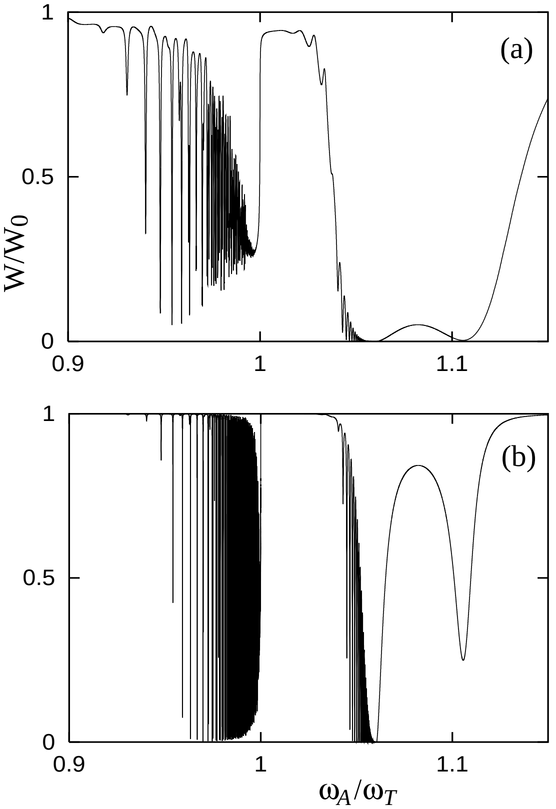

Figure 11: The fraction of emitted radiation energy in spontaneous decay of an excited atom placed near a microsphere is shown as a function of the transition frequency for a radially oriented transition dipole moment and a single-resonance Drude–Lorentz-type dielectric [$R = 2\,\lambda_T$; $\omega_P = 0.5\,\omega_T$; $\gamma/\omega_T = 10^{-4}$; $\Delta r = 0.02\,\lambda_T$; $\gamma/\omega_T = 10^{-4}$ (a), 10^{-6} (b). [After Ho *et al.* (2001).]

$$\frac{W}{W_0} = \frac{3\Gamma_0}{2\Gamma^{\perp}} \sum_{l=1}^{\infty} \frac{l(l+1)(2l+1)}{(k_A r_A)^2} \times \left| j_l(k_A r_A) + \mathcal{B}_l^N(\omega_A) h_l^{(1)}(k_A r_A) \right|^2. \qquad (7.12)$$

Recall that $W/W_0 = 1$ implies fully radiative decay, while $W/W_0 = 0$ implies fully nonradiative one.

The dependence of the ratio W/W_0 on the atomic transition frequency is illustrated in Fig. 11. The minima at the WG field resonance frequencies indicate that the nonradiative decay is enhanced relative to the radiative one. Obviously, photons at these frequencies are captured inside the microsphere for some time, and hence the probability of photon absorption is increased. For transition frequencies inside a band gap, two regions can be distinguished. In the low-frequency region, where low-order SG waves are typically excited, radiative decay dominates. Here, the light penetration depth into the sphere is small and the probability of a photon being absorbed is small as well. With increasing atomic transition frequency the penetration depth increases and the chance of a photon to escape drastically diminishes. As a result, nonradiative decay dominates. Clearly, the strength of the effect decreases with decreasing material absorption [compare Fig. 11(a) with (b)].

From the figure two well pronounced minima of the totally emitted light energy, i.e., noticeable maxima of the energy transfer to the matter, are seen for transition frequencies inside the band gap. The first minimum results from the overlapping high-order SG waves that mainly underly absorption losses. The second one is observed at the longitudinal resonance frequency of the medium. It can be attributed to the atomic near-field interaction with the longitudinal component of the medium-assisted electromagnetic field, the strength of the longitudinal field resonance being proportional to ε_I. Hence, the dip at the longitudinal frequency of the emitted radiation energy reduces with decreasing material absorption and may disappear when the atom is moved sufficiently away from the surface.

7.3.3 Temporal evolution

Throughout this section we have restricted our attention to the weak-coupling regime where the excited atomic state decays exponentially, Eq. (3.21). When retardation is disregarded, then the intensity of the emitted light (at some chosen space point) simply decreases exponentially, Eq. (3.34). To study the effect of retardation, the frequency integral in the exact equation (3.29) must be performed numerically in general.

Typical examples of the temporal evolution of the far-field intensity are shown in Fig. 12 for a radially oriented transition dipole moment in the case when the atomic transition frequency coincides with the frequency of a WG wave. Whereas the long-time behavior of the intensity of the emitted light is, with little error, exponential, the short-time behavior (on a time scale given by the atomic decay time) sensitively depends on the quality factor [$Q \sim 10^3$ in Fig. 12(a), $Q \sim 10^4$ in Fig. 12(b)]. The observed delay between the upper-state atomic population and the intensity of the emitted light can be quite large for a high-Q microsphere, because the

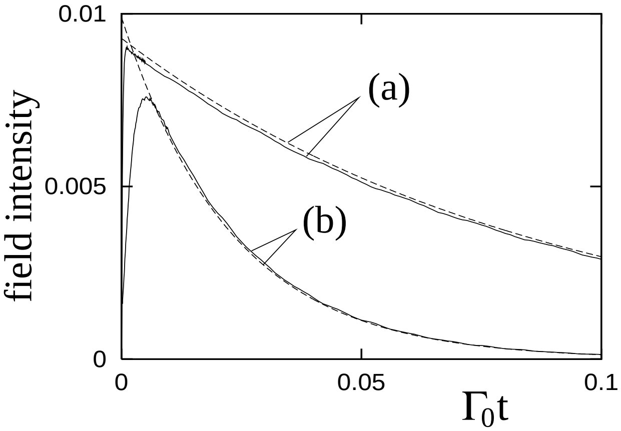

Figure 12: Exact (solid lines) and approximate (dashed lines) temporal evolution of the far-field intensity $I(\mathbf{r},t)/(k_A^3 d/4\pi\varepsilon_0)^2$ at a fixed point of observation of a radially oscillating dipole near a single-resonance Drude–Lorentz-type dielectric microsphere [$R=2\,\lambda_T$; $\omega_P=0.5\,\omega_T$; $\gamma/\omega_T=10^{-4}$; $\Delta r=0.02\,\lambda_T$; $r=20\,\lambda_T$; $\theta=3$; $\Gamma_0/\omega_T=10^{-7}$; $\omega_A=0.91779\,\omega_T$ (a), $0.94042\,\omega_T$ (b). [After Ho *et al.* (2001).]

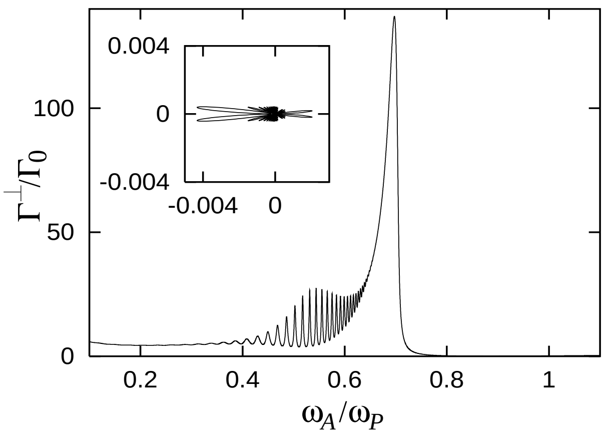

Figure 13: The decay rate of an atom near a metallic microsphere is shown as a function of the transition frequency for a radially oriented transition dipole moment and a single-resonance metal of Drude type [$R=5\lambda_P$; $\gamma/\omega_P=0.005$; $\Delta r=0.1\,\lambda_P$. Inset: polar diagram of the far-field emission pattern $|\mathbf{F}^{\perp}(\mathbf{r},\mathbf{r}_A,\omega_A)|^2/(k_A^3\mu/4\pi\epsilon_0)^2$ for $r=50\,\lambda_P$ and $\omega_A/\omega_P=0.5026$. [After Ho *et al.* (2001).]

time that a photon spends in the sphere increases with the Q value. Further, in the short-time domain some kink-like fine structure is observed, which obviously reflects the different arrival times associated with multiple reflections.

7.4 Metallic Microsphere

The permittivity of a metal (on the basis of the Drude model) can be obtained by setting in Eq. (4.1) the lowest resonance frequency $\omega_{T\alpha}$ equal to zero. Thus, the results derived for the band gap of a dielectric microsphere also apply, for appropriately chosen values of the corresponding $\omega_{P\alpha}\equiv\omega_P$ and $\gamma_\alpha\equiv\gamma$, to a metallic sphere. In particular, the results obtained in the nonretardation limit ($c\to\infty$) and for small sphere sizes ($R\ll\lambda_P$) [Ruppin (1982); Agarwal *et al.* (1983)] are recovered.

The dependence of the decay rate on the transition frequency of an excited atom near a metallic microsphere is illustrated in Fig. 13 for $R>\lambda_P$. The inset shows the emission pattern for the case when the atomic transition frequency coincides with the frequency of a SG wave. Note that the SG field resonances seen in Fig. 13 obey, according to condition (4.10), the relation $\omega/\omega_P<1/\sqrt{2}\simeq0.71$. When the radius of the microsphere becomes substantially smaller than the wavelength λ_P, then distinct peaks are only seen for a few lowest-order resonances [Ruppin (1982); Agarwal *et al.* (1983)]. It is worth noting that, in contrast to dielectric matter, a large absorption in metals can substantially enhance the near-surface divergence of the decay rate, Eq. (5.8), which is in agreement with experimental observations of the fluorescence from dye molecules near a planar metal surface [Drexhage (1974)].

8 QUANTUM CORRELATIONS

Let us finally address the problem of spontaneous decay of an atom in the case when there is a second atom that is resonantly dipole-dipole coupled to the first one. Similarly to single-atom spontaneous decay, the dipole-dipole interaction can be controlled by the presence of macroscopic bodies. Various aspects of the problem have been discussed for bulk material [Knoester *et al.* (1989)], photonic crystals [Kurizki *et al.* (1988); Kurizki (1990); John *et al.* (1995); Bay *et al.* (1997); Rupasov *et al.* (1997)], optical lattices [Goldstein *et al.* (1997b); Guzman *et al.* (1998)], planar cavities [Kobayashi *et al.* (1995a); Agarwal *et al.* (1998)] (and unspecified cavities [Kurizki *et al.* (1996); Goldstein *et al.* (1997a)]), and microspheres [Agarwal *et al.* (2000)]. In particular, resonant energy transfer realized through dipole-dipole interaction has been studied theoretically for bulk material [Juzeliūnas *et al.* (1994a,b)], microspheres [Gersten *et al.* (1984); Druger *et al.* (1987); Leung *et al.* (1988)], and planar microcavities [Kobayashi *et al.* (1995a,b)], and experimentally for droplets [Folan *et al.* (1985)] and planar microstructures [Hopmeier *et al.* (1999); Andrew *et al.* (2000)], with potential for enhanced photon-harvesting systems and optical networks.

Interatomic interaction can give rise to nonclassical correlation and may be used for entangled-state preparation, which has been of increasing interest in the study of fundamental issues of quantum mechanics and with regard to application in quantum information processing. The entanglement, which is very weak in free space, may be expected to be enhanced significantly in resonator-like equipments. Proposals have been made for entangling spatially separated atoms in Jaynes-Cummings systems through sequential or simultaneous strong atom-field coupling [Kudryavtsev *et al.* (1993); Phoenix *et al.* (1993); Cirac *et al.* (1994); Freyberger *et al.* (1996); Gerry (1996); Plenio *et al.* (1999); Beige *et al.* (2000)].

Unfortunately, the Jaynes-Cummings model does not give any indication of the influence on entanglement of the actual properties (such as form and intrinsic dispersion and absorption) of the bodies in a really used scheme. From Section 3.3 we know that not only the evolution of a single atom but also the mutual evolution of two atoms is fully determined by the Green tensor according to the chosen configuration of macroscopic bodies. The formalism thus renders it possible to examine interatom quantum correlations established in the presence of arbitrary macroscopic body.

8.1 Entangled-state preparation

Weak Coupling Let us consider, e.g., two atoms near a microsphere of the type studied in Section 7. To be more specific, let as assume that the (two-level) atoms are of the same kind, that they are located at diametrically opposite positions ($\mathbf{r}_A = -\mathbf{r}_B$), and that their transition dipole moments are radially oriented.

Obviously, the conditions (3.44) and (3.45) are fulfilled for such a system, so that from Eqs. (3.51) and (3.53) together with the Green tensor for a microsphere (Appendix A.2) one then finds that

$$\Gamma^{\perp}_{\pm} = \tfrac{3}{2}\Gamma_0 \sum_{l=1}^{\infty} \mathrm{Re}\biggl\{ \frac{l(l+1)(2l+1)}{(k_A r_A)^2} \times \Bigl[j_l(k_A r_A) + \mathcal{B}^N_l(\omega_A) h^{(1)}_l(k_A r_A) \Bigr] \times h^{(1)}_l(k_A r_A) \Bigl[1 \mp (-1)^l \Bigr] \biggr\}. \tag{8.1}$$

When atom A is initially in the upper state and atom B is accordingly in the lower state, then the two superposition states $|+\rangle$ and $|-\rangle$, Eq. (3.49), are initially equally excited $[C_+(0) = C_-(0) = 2^{-\frac{1}{2}}]$. If the atomic transition frequency coincides with a microsphere resonance, the most significant contribution to the single-atom decay rate $\Gamma^{\perp}$, Eq. (7.1), comes (for sufficiently small atom-surface distance) from the corresponding term in the l-sum, i.e.,

$$\Gamma^{\perp} \simeq \tfrac{3}{2}\Gamma_0\, l(l+1)(2l+1) \times \mathrm{Re}\biggl\{ \biggl[\frac{h^{(1)}_l(k_A r_A)}{k_A r_A} \biggr]^2 \mathcal{B}^N_l(\omega_A) \biggr\}, \tag{8.2}$$

and Eq. (8.1) can be approximated as follows:

$$\Gamma^{\perp}_{\pm} \simeq \Gamma^{\perp} \Bigl[1 \mp (-1)^l \Bigr]. \tag{8.3}$$

Hence $\Gamma_- \gg \Gamma_+$ ($\Gamma_+ \gg \Gamma_-$) if l is even (odd), i.e., the state $|-\rangle$ ($|+\rangle$) decays much faster than the state $|+\rangle$ ($|-\rangle$).

Consequently, there exists a time window, during which the overall system is prepared in an entangled state that is a superposition of the state with the atoms being in the state $|+\rangle$ ($|-\rangle$) and the medium-assisted field being in the ground state, and all the states with the atoms being in the lower state $|L\rangle$ and the medium-assisted field being in a single-quantum Fock state. The window is opened when the state $|-\rangle$ ($|+\rangle$) has already decayed while the state $|L\rangle$ emerges, and it is closed roughly after the lifetime of the state $|+\rangle$ ($|-\rangle$). As a result, the two atoms are also entangled to each other. The state is a statistical mixture, the density operator of which is obtained from the density operator of the overall system by taking the trace with respect to the medium-assisted field. Within approximation (8.3) it takes the form of

$$\hat{\rho}_A \simeq |C_{\pm}(t)|^2 |\pm\rangle\langle\pm| + \bigl[1 - |C_{\pm}(t)|^2\bigr] |L\rangle\langle L|, \tag{8.4}$$

where

$$C_{\pm}(t) \simeq 2^{-1/2} e^{-\Gamma_{\pm} t}. \tag{8.5}$$

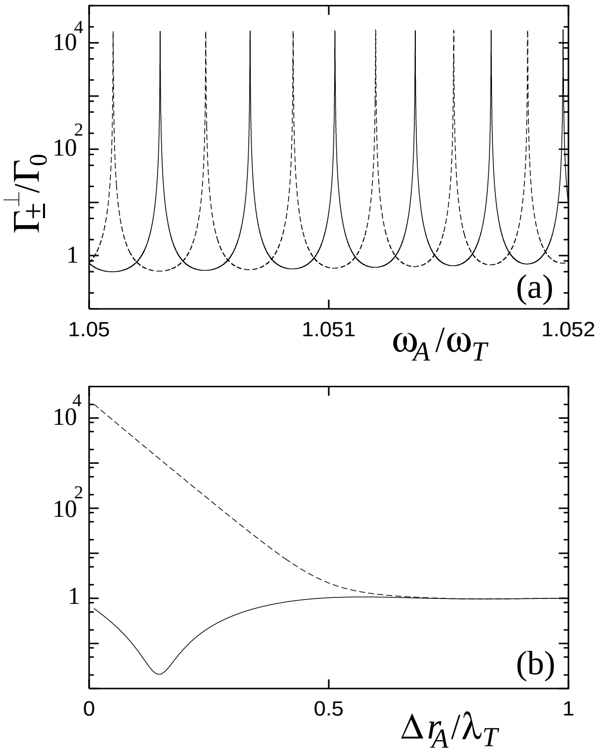

Figure 14: The dependence of the decay rates Γ_+ (solid line) and Γ_- (dashed line) on (a) the transition frequency and (b) the distance of the atoms from a microsphere is shown for two atoms at (with respect to a sphere) diametrically opposite positions, radially oriented transition dipole moments, and a single-resonance Drude–Lorentz-type dielectric [$R = 10\,\lambda_T$; $\omega_P = 0.5\,\omega_T$; $\gamma = 10^{-6}\omega_T$; $\Delta r_B = \Delta r_A \geq 10^{-2}\,\lambda_T$; (a) $\Delta r_A = 0.02\,\lambda_T$; (b) $\omega_A \simeq 1.0501\,\omega_T$].

Applying the criterion suggested by Peres (1996), it is not difficult to prove that the state (8.4) is indeed inseparable. It is worth noting that the atoms become entangled within the weak-coupling regime, starting from the state $|U_A\rangle$ (or $|U_B\rangle$) and the vacuum field. In the language of (Markovian) damping theory one would probably say that the two atoms are coupled to the same dissipative system, which gives rise to the quantum coherence.

The frequency dependence of $\Gamma_\pm$ as given by Eq. (8.1) is illustrated in Fig. 14(a) for a frequency interval inside a band gap, and the dependence on the atom-surface distance is illustrated in Fig. 14(b). We see that the values of Γ_+ and Γ_- can be substantially different from each other before they tend to the free-space rate Γ_0 as the distance from the sphere becomes sufficiently large. In particular, the decay of one of the states $|+\rangle$ or $|-\rangle$ can strongly be suppressed [see the minimum value of Γ_+ in Fig. 14(b)] at the expense of the other one, which rapidly decays. Note that Γ_+ also differs from Γ_- for two atoms in free space [DeVoe *et al.* (1996)]. However, the difference that occurs by mediation of the microsphere is much larger. For example, at the distance for which in Fig. 14(b) Γ_+ attains the minimum the ratio $\Gamma_-/\Gamma_+ \simeq 67000$ is observed, which is to be compared with the free-space ratio $\Gamma_-/\Gamma_+ \simeq 1.0005$. The effect may become even more pronounced for larger microsphere sizes and lower material absorption, i.e., sharper microsphere resonances. Needless to say that it is not only observed for SG waves considered in Fig. 14, but also for WG waves.

Strong Coupling Entangled-state preparation in the weak-coupling regime has the advantage that it could routinely be achieved experimentally. However, the value of $|C_+(t)|^2$ in Eq. (8.4) (or the value of $|C_-(t)|^2$ in the corresponding equation for the state $|-\rangle$) is always less than 1/2. In order to achieve a higher degree of entanglement, the strong-coupling regime is required.

Let us assume that the two atoms are initially in the ground state and the medium-assisted field is excited. The field excitation can be achieved, for example, by coupling an excited atom D to the microsphere and then making sure that the atomic excitation is transferred to the field (cf. Section 3.1). If the atom D strongly interacts with the field, the excitation transfer can be controlled by adjusting the interaction time. Another possibility would be measuring the state populations and discarding the events where the atom is found in the upper state. Here we restrict our attention to the first method and assume that all three atoms D, A, and B strongly interact with the same microsphere resonance (of mid-frequency ω_C and line width $\Delta\omega_C$). According to Eq. (3.26), the upper-state probability amplitude $C_{U_D}(t)$ of atom D reads

$$C_{U_D}(t) = e^{-\Delta\omega_C(t+\Delta t)/2} \cos[\Omega_D(t+\Delta t)/2], \quad (8.6)$$

with Ω_D being given according to Eq. (3.27). For

$$\Delta t = \pi/\Omega_D, \quad (8.7)$$

the initially (i.e., at time $t = -\Delta t$) excited atom D is at time $t = 0$ in the lower state [$C_{U_D}(0) = 0$].

From the preceding subsection we know that when the resonance angular-momentum number l

is odd (even), then the state $|+\rangle$ ($|-\rangle$) "feels" a sharply peaked high density of medium-assisted field states, so that a strong-coupling approximation of the type (3.24) applies. The state $|-\rangle$ ($|+\rangle$), in contrast, "feels" a flat one and the (weak-coupling) Markov approximation applies. Assuming atom A (or B) is at the same position as was atom D, from Eqs. (3.47), (8.6), and (8.7) we then find that

$$C_{\pm}(t) \simeq -e^{-\Delta\omega_C(t+\pi/\Omega_D)/2} \sin(\Omega_{\pm}t/2) \qquad (8.8)$$

[with $\Omega_{\pm}$ according to Eq. (3.27)] and

$$C_{\mp}(t) \simeq 0 \qquad (8.9)$$

(the sign of $C_-(t)$ in Eq. (8.8) is reversed if atom B is at the same position as was atom D). Note that $\Omega_{\pm} = 2^{\frac{1}{2}}\Omega$, because of Eq. (8.3). The two-atom entangled state is again of the form given in Eq. (8.4), but now the weight of the state $|+\rangle$ ($|-\rangle$) can reach values larger 1/2, provided that the resonance linewidth $\Delta\omega_C$ is small enough.

8.2 Violation of Bell's inequality

Violations of Bell's inequalities provide support to quantum mechanics versus local (hidden-variables) theories [Bell (1965); Clauser *et al.* (1969)]. Despite outstanding progress[5] in the test of Bell's inequalities, a decisive experiment to rule out any local realistic theory is yet to be performed [Vaidman (2001)], and the problem continues to attract much attention. Though entangled states of spatially separated atoms in a cavity have been observed [Hagley *et al.* (1997)], a test of Bell's inequalities for such a system has yet to be realized.

The Bell's inequality for spin systems can be written in the form of [Bell (1965); Clauser *et al.* (1969)]

$$\begin{aligned} B_S = |E(\theta_1,\theta_2) - E(\theta_1,\theta_2') \\ + E(\theta_1',\theta_2) + E(\theta_1',\theta_2')| \le 2, \end{aligned} \qquad (8.10)$$

where

$$E(\theta_1,\theta_2) = \langle \hat{\sigma}_A^{\theta_1} \hat{\sigma}_B^{\theta_2} \rangle, \qquad (8.11)$$

$$\hat{\sigma}_A^{\theta} = \cos\theta\, \hat{\sigma}_A^x + \sin\theta\, \hat{\sigma}_A^y. \qquad (8.12)$$

When the atomic state $|u_A, u_B\rangle$ is not populated, as it is the case for a state of the type (8.4), it is not difficult to prove that

$$E(\theta_1,\theta_2) = E(\theta_1-\theta_2, 0). \qquad (8.13)$$

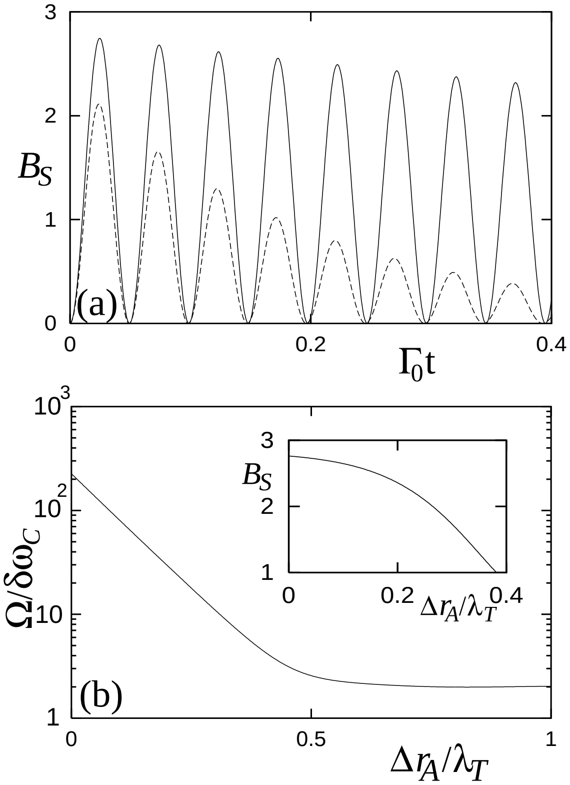

Figure 15: The dependence on time of B_S is shown for two atoms at (with respect to a microsphere) diametrically opposite positions, radially oriented transition dipole moments, and a single-resonance Drude–Lorentz-type dielectric [$R = 10\,\lambda_T$; $\omega_P = 0.5\,\omega_T$; $\Delta r_B = \Delta r_A = 0.02\,\lambda_T$; $\omega_A = 1.0501\,\omega_T$; $\Gamma_0 = 10^{-6}\,\omega_T$; $\Omega_D = \Omega$; $\gamma/\omega_T = 10^{-6}$ (solid line), 10^{-5} (dashed line)]. (b) $\Omega/\Delta\omega_C$ versus Δr_A for $\gamma/\omega_T = 10^{-6}$ ($\Delta r_A \ge 10^{-3}\,\lambda_T$). The inset shows the variation of the first maximum value of B_S in (a).

Let us choose

$$\theta = \theta_1 - \theta_2 = \theta_2 - \theta_1' = \theta_1' - \theta_2'\,. \qquad (8.14)$$

The inequality (8.10) thus simplifies to

$$B_S = |3E(\theta,0) - E(3\theta,0)| \le 2. \qquad (8.15)$$

An entangled state of the type (8.4) can only give rise to a violation of the Bell's inequality if $|C_+(t)|^2 \ge 2^{-\frac{1}{2}} \simeq 0.71$ [Beige *et al.* (2000)], which cannot be achieved in the weak-coupling regime, Eq. (8.5). It can be achieved, in contrast, in the strong-coupling regime, Eq. (8.8), where

---

[5] For recent experiments using photons, see Weihs *et al.* (1998); Kuzmich *et al.* (2000), and using trapped ions, see Rowe *et al.* (2001).

$$E(\theta,0) = \cos\theta\,|C_\pm(t)|^2 = \cos\theta\, e^{-\Delta\omega_C(t+\pi/\Omega_D)} \sin^2\!\big(\Omega t/\sqrt{2}\big). \tag{8.16}$$

Substitution of this expression into in Eq. (8.15) yields, on choosing $\theta = \pi/4$,

$$B_S = 2\sqrt{2}\, e^{-\Delta\omega_C(t+\pi/\Omega_D)} \sin^2\!\big(\Omega t/\sqrt{2}\big), \tag{8.17}$$

which clearly shows that $B_S > 2$ becomes possible as long as $\Delta\omega_C(t+\pi/\Omega_D) \ll 1$. Examples of the temporal evolution of B_S for two atoms near a dielectric microsphere are shown in Fig. 15(a). In Figure 15(b) the dependence of the ratio $\Omega/\Delta\omega_C$ on the distance of the atoms from the sphere is plotted. The strong-coupling regime can be observed for distances for which $\Omega/\Delta\omega_C \gg 1$ is valid. The inset reveals that the maximum value of B_S decreases with increasing atom-surface distance and reduces below the threshold value of 2 still in the strong-coupling regime.

9 SUMMARY

We have studied spontaneous decay in the presence of dispersing and absorbing macroscopic bodies, basing on quantization of the (macroscopic) electromagnetic field in arbitrary linear, causal media. The formalism covers both weak and strong couplings and enables one to include the material absorption and dispersion in a consistent way, without restriction to a particular frequency domain. It replaces the standard concept of orthogonal-mode decomposition, which requires real permittivities and thus does not allow for material absorption, with a source-quantity representation in terms of the classical Green tensor and appropriately chosen bosonic-field variables. All relevant information about the bodies such as form and intrinsic dispersion and absorption properties are contained in the Green tensor.

The formalism has been applied to study spontaneous decay of a single atom in the presence of various absorbing and dispersing macroscopic bodies, including open configurations such as bulk and planar half space media, and closed configurations such as a spherical cavity or a microsphere. Absorption can noticeably influence spontaneous decay. So, the decay rate in absorbing bulk material takes a much more complicated form than one would expect from the simple product form that is commonly used for nonabsorbing matter. The decay rate of an atom located very near a planar surface shows that due to material absorption the decay rate drastically rises as the atom approaches the surface of the body, because of near-field assisted (nonradiative) energy transfer from the atom to the medium. In fact, this is valid for an atom that is sufficiently near an arbitrary body, because for short enough atom–surface distances, any curved surface can be approximated by a planar one.

Spontaneous decay can strongly be influenced by field resonances that can appear due to the presence of macroscopic bodies, depending on whether the atomic transition frequency is tuned to a field resonance or not. In particular, the decay process can be mainly radiative or nonradiative, which depends on whether the radiative losses due to input-output coupling or the losses due to material absorption dominate. In particular, to understand what happens when the atomic transition frequency is inside a band-gap zone of a body, inclusion in the study of material absorption is necessary.

Finally, spontaneous decay of (two) dipole-dipole coupled atoms in the presence of macroscopic bodies offers the possibility of entangled state preparation and verification of the violation of Bell's inequalities. Whereas entangled states can already be prepared in the weak-coupling regime, violation of Bell's inequalities requires the strong-coupling regime, the ultimate limits being given by material absorption.

ACKNOWLEDGMENTS

We thank S. Scheel, E. Schmidt, and A. Tip for discussions. H.T.D. gratefully acknowledges support from the Alexander von Humboldt Stiftung. This work was supported by the Deutsche Forschungsgemeinschaft.

A THE GREEN TENSOR

A.1 Bulk Medium

For bulk material the Green tensor reads as ($\boldsymbol{\rho} = \mathbf{r} - \mathbf{r}'$)

$$\boldsymbol{G}(\mathbf{r},\mathbf{r}',\omega) = \left[\boldsymbol{\nabla}^r \otimes \boldsymbol{\nabla}^r + \boldsymbol{I} q^2(\omega)\right] \frac{\mathrm{e}^{iq(\omega)\rho}}{4\pi q^2(\omega)\rho}\,, \tag{A.1}$$

where

$$q(\omega) \;=\; \sqrt{\varepsilon(\omega)}\,\omega/c. \tag{A.2}$$

It can be decomposed into a longitudinal and a transverse part,

$$\boldsymbol{G}(\mathbf{r},\mathbf{r}',\omega) = \boldsymbol{G}^{\|}(\mathbf{r},\mathbf{r}',\omega) + \boldsymbol{G}^{\perp}(\mathbf{r},\mathbf{r}',\omega), \qquad \text{(A.3)}$$

where

$$\boldsymbol{G}^{\|}(\mathbf{r},\mathbf{r}',\omega) = -\frac{1}{4\pi q^2}\left[\frac{4\pi}{3}\delta(\boldsymbol{\rho})\boldsymbol{I} + \left(\boldsymbol{I} - \frac{3\boldsymbol{\rho}\otimes\boldsymbol{\rho}}{\rho^2}\right)\frac{1}{\rho^3}\right] \qquad \text{(A.4)}$$

and

$$\boldsymbol{G}^{\perp}(\mathbf{r},\mathbf{r}',\omega) = \frac{1}{4\pi q^2}\left\{\left(\boldsymbol{I} - \frac{3\boldsymbol{\rho}\otimes\boldsymbol{\rho}}{\rho^2}\right)\frac{1}{\rho^3} + q^3\left[\left(\frac{1}{q\rho} + \frac{i}{(q\rho)^2} - \frac{1}{(q\rho)^3}\right)\boldsymbol{I} - \left(\frac{1}{q\rho} + \frac{3i}{(q\rho)^2} - \frac{3}{(q\rho)^3}\right)\frac{\boldsymbol{\rho}\otimes\boldsymbol{\rho}}{\rho^2}\right]\mathrm{e}^{iq\rho}\right\}. \qquad \text{(A.5)}$$

In particular, from Eq. (A.5) it follows that

$$\operatorname{Im}\boldsymbol{G}^{\perp}(\mathbf{r},\mathbf{r},\omega) = \lim_{\mathbf{r}'\to\mathbf{r}}\operatorname{Im}\boldsymbol{G}^{\perp}(\mathbf{r},\mathbf{r}',\omega) = \frac{\omega}{6\pi c}\,n_R(\omega)\boldsymbol{I}. \qquad \text{(A.6)}$$

A.2 Spherical Multilayers

The Green tensor of a spherical structure, consisting of $\mathcal{N}$ concentric layers, enumerated from outward in (the outmost layer labeled as layer 1, the innermost layer as layer $\mathcal{N}$), can be decomposed into two parts

$$\boldsymbol{G}(\mathbf{r},\mathbf{r}',\omega) = \boldsymbol{G}^{(s)}(\mathbf{r},\mathbf{r}',\omega)\delta_{fs} + \boldsymbol{G}^{(fs)}(\mathbf{r},\mathbf{r}',\omega), \qquad \text{(A.7)}$$

where $\boldsymbol{G}^{(s)}(\mathbf{r},\mathbf{r}',\omega)$ represents the contribution of the direct waves from the source in an unbounded space, and $\boldsymbol{G}^{(fs)}(\mathbf{r},\mathbf{r}',\omega)$ is the scattering part that describes the contribution of the multiple reflection $(f=s)$ and transmission $(f\neq s)$ due to the presence of the surfaces of discontinuity (f and s, respectively, refer to the regions where are the field and source points $\mathbf{r}$ and $\mathbf{r}'$). In Eq. (A.7), $\boldsymbol{G}^{(s)}$ is nothing but the bulk-material Green tensor (A.1). In the (local) spherical coordinate systems it reads as [see, e.g., Li *et al.* (1994)]

$$\boldsymbol{G}^{(s)}(\mathbf{r},\mathbf{r}',\omega) = \frac{\mathbf{e}_r\otimes\mathbf{e}_r}{k_s^2}\,\delta(r-r') + \frac{ik_s}{4\pi}\sum_{\substack{e\\o}}\sum_{l=1}^{\infty}\sum_{m=0}^{l}\left\{\frac{2l+1}{l(l+1)}\frac{(l-m)!}{(l+m)!}(2-\delta_{0m}) \times\left[\mathbf{M}^{(1)}_{\substack{e\\o}lm}(\mathbf{r},k_s)\otimes\mathbf{M}_{\substack{e\\o}lm}(\mathbf{r}',k_s) + \mathbf{N}^{(1)}_{\substack{e\\o}lm}(\mathbf{r},k_s)\otimes\mathbf{N}_{\substack{e\\o}lm}(\mathbf{r}',k_s)\right]\right\} \qquad \text{(A.8)}$$

if $r\geq r'$, and $\boldsymbol{G}^{(s)}(\mathbf{r},\mathbf{r}',\omega) = \boldsymbol{G}^{(s)}(\mathbf{r}',\mathbf{r},\omega)$ if $r<r'$. The scattering part $\boldsymbol{G}^{(fs)}(\mathbf{r},\mathbf{r}',\omega)$ in Eq. (A.7) reads [Li *et al.* (1994)]

$$\begin{aligned}\boldsymbol{G}^{(fs)}&(\mathbf{r},\mathbf{r}',\omega)\\ &= \frac{ik_s}{4\pi}\sum_{\substack{e\\o}}\sum_{l=1}^{\infty}\sum_{m=0}^{l}\left(\frac{2l+1}{l(l+1)}\frac{(l-m)!}{(l+m)!}(2-\delta_{0m})\right.\\ &\left\{(1-\delta_{f\mathcal{N}})\mathbf{M}^{(1)}_{\substack{e\\o}lm}(\mathbf{r},k_f)\otimes\left[\mathbf{M}_{\substack{e\\o}lm}(\mathbf{r}',k_s)\right.\right.\\ &\times(1-\delta_{s1})\mathcal{A}^M_l(\omega) + \left.\mathbf{M}^{(1)}_{\substack{e\\o}lm}(\mathbf{r}',k_s)(1-\delta_{s\mathcal{N}})\mathcal{B}^M_l(\omega)\right]\\ &+(1-\delta_{f\mathcal{N}})\mathbf{N}^{(1)}_{\substack{e\\o}lm}(\mathbf{r},k_f)\otimes\left[\mathbf{N}_{\substack{e\\o}lm}(\mathbf{r}',k_s)\right.\\ &\times(1-\delta_{s1})\mathcal{A}^N_l(\omega) + \left.\mathbf{N}^{(1)}_{\substack{e\\o}lm}(\mathbf{r}',k_s)(1-\delta_{s\mathcal{N}})\mathcal{B}^N_l(\omega)\right]\\ &+(1-\delta_{f1})\mathbf{M}_{\substack{e\\o}lm}(\mathbf{r},k_f)\otimes\left[\mathbf{M}_{\substack{e\\o}lm}(\mathbf{r}',k_s)\right.\\ &\times(1-\delta_{s1})\mathcal{C}^M_l(\omega) + \left.\mathbf{M}^{(1)}_{\substack{e\\o}lm}(\mathbf{r}',k_s)(1-\delta_{s\mathcal{N}})\mathcal{D}^M_l(\omega)\right]\\ &+(1-\delta_{f1})\mathbf{N}_{\substack{e\\o}lm}(\mathbf{r},k_f)\otimes\left[\mathbf{N}_{\substack{e\\o}lm}(\mathbf{r}',k_s)\right.\\ &\times(1-\delta_{s1})\mathcal{C}^N_l(\omega)\\ &\left.\left.\left.+\mathbf{N}^{(1)}_{\substack{e\\o}lm}(\mathbf{r}',k_s)(1-\delta_{s\mathcal{N}})\mathcal{D}^N_l(\omega)\right]\right\}\right),\end{aligned} \qquad \text{(A.9)}$$

where

$$k_{f(s)} = \sqrt{\varepsilon_{f(s)}(\omega)}\,\frac{\omega}{c}\,, \qquad \text{(A.10)}$$

and $\mathbf{M}$ and $\mathbf{N}$ represent TM- and TE-waves, respectively,

$$\mathbf{M}_{\substack{e\\o}nm}(\mathbf{r},k) = \mp\frac{m}{\sin\theta}j_n(kr)P_n^m(\cos\theta)\binom{\sin}{\cos}(m\phi)\mathbf{e}_\theta - j_n(kr)\frac{dP_n^m(\cos\theta)}{d\theta}\binom{\cos}{\sin}(m\phi)\mathbf{e}_\phi\,, \qquad \text{(A.11)}$$

$$\mathbf{N}_{\substack{e\\o}nm}(\mathbf{r},k) = \frac{n(n+1)}{kr}j_n(kr)P_n^m(\cos\theta)\binom{\cos}{\sin}(m\phi)\mathbf{e}_r + \frac{1}{kr}\frac{d[rj_n(kr)]}{dr}\left[\frac{dP_n^m(\cos\theta)}{d\theta}\binom{\cos}{\sin}(m\phi)\mathbf{e}_\theta \mp\frac{m}{\sin\theta}P_n^m(\cos\theta)\binom{\sin}{\cos}(m\phi)\mathbf{e}_\phi\right], \qquad \text{(A.12)}$$

with $j_n(x)$ being the spherical Bessel function of the first kind and $P_n^m(x)$ being the associated Legendre function. The superscript (1) in Eq. (A.9) indicates that in Eqs. (A.11) and (A.12) the spherical Bessel function $j_n(x)$ has to be replaced by the first-type spherical Hankel function $h_n^{(1)}(x)$.

The coefficients $\mathcal{A}_l^{M,N}$, $\mathcal{B}_l^{M,N}$, $\mathcal{C}_l^{M,N}$, and $\mathcal{D}_l^{M,N}$ are to be found from the coupled recurrence equations

$$\begin{aligned} &\begin{pmatrix} \mathcal{A}_{(f+1)s}^{M,N} + \delta_{(f+1)s} & \mathcal{B}_{(f+1)s}^{M,N} \\ \mathcal{C}_{(f+1)s}^{M,N} & \mathcal{D}_{(f+1)s}^{M,N} \end{pmatrix} \\ &\quad = \begin{pmatrix} 1/T_{Ff}^{M,N} & R_{Ff}^{M,N}/T_{Ff}^{M,N} \\ R_{Pf}^{M,N}/T_{Pf}^{M,N} & 1/T_{Pf}^{M,N} \end{pmatrix} \\ &\qquad \times \begin{pmatrix} \mathcal{A}_{fs}^{M,N} & \mathcal{B}_{fs}^{M,N} \\ \mathcal{C}_{fs}^{M,N} & \mathcal{D}_{fs}^{M,N} + \delta_{fs} \end{pmatrix}, \end{aligned} \tag{A.13}$$

$$\mathcal{A}_{\mathcal{N}s}^{M,N} = \mathcal{B}_{\mathcal{N}s}^{M,N} = \mathcal{C}_{1s}^{M,N} = \mathcal{D}_{1s}^{M,N} = 0 \tag{A.14}$$

[with f and s being taken according to Eq. (A.9)]. Here, the coefficients are redefined as

$$\begin{aligned} &\mathcal{A}_l^{M,N} \equiv \mathcal{A}_{fs}^{M,N},\ \mathcal{B}_l^{M,N} \equiv \mathcal{B}_{fs}^{M,N}, \\ &\mathcal{C}_l^{M,N} \equiv \mathcal{C}_{fs}^{M,N},\ \mathcal{D}_l^{M,N} \equiv \mathcal{D}_{fs}^{M,N}, \end{aligned} \tag{A.15}$$

and

$$R_{Pf}^{M} = \frac{k_{f+1}H'_{(f+1)f}H_{ff} - k_f H'_{ff}H_{(f+1)f}}{k_{f+1}J_{ff}H'_{(f+1)f} - k_f J'_{ff}H_{(f+1)f}}, \tag{A.16}$$

$$R_{Ff}^{M} = \frac{k_{f+1}J'_{(f+1)f}J_{ff} - k_f J'_{ff}J_{(f+1)f}}{k_{f+1}J'_{(f+1)f}H_{ff} - k_f J_{(f+1)f}H'_{ff}}, \tag{A.17}$$

$$R_{Pf}^{N} = \frac{k_{f+1}H_{(f+1)f}H'_{ff} - k_f H_{ff}H'_{(f+1)f}}{k_{f+1}J'_{ff}H_{(f+1)f} - k_f J_{ff}H'_{(f+1)f}}, \tag{A.18}$$

$$R_{Ff}^{N} = \frac{k_{f+1}J_{(f+1)f}J'_{ff} - k_f J_{ff}J'_{(f+1)f}}{k_{f+1}J_{(f+1)f}H'_{ff} - k_f J'_{(f+1)f}H_{ff}}, \tag{A.19}$$

$$T_{Pf}^{M} = \frac{k_{f+1}[J_{(f+1)f}H'_{(f+1)f} - J'_{(f+1)f}H_{(f+1)f}]}{k_{f+1}J_{ff}H'_{(f+1)f} - k_f J'_{ff}H_{(f+1)f}}, \tag{A.20}$$

$$T_{Ff}^{M} = \frac{k_{f+1}[J'_{(f+1)f}H_{(f+1)f} - J_{(f+1)f}H'_{(f+1)f}]}{k_{f+1}J'_{(f+1)f}H_{ff} - k_f J_{(f+1)f}H'_{ff}}, \tag{A.21}$$

$$T_{Pf}^{N} = \frac{k_{f+1}[J'_{(f+1)f}H_{(f+1)f} - J_{(f+1)f}H'_{(f+1)f}]}{k_{f+1}J'_{ff}H_{(f+1)f} - k_f J_{ff}H'_{(f+1)f}}, \tag{A.22}$$

$$T_{Ff}^{N} = \frac{k_{f+1}[J_{(f+1)f}H'_{(f+1)f} - J'_{(f+1)f}H_{(f+1)f}]}{k_{f+1}J_{(f+1)f}H'_{ff} - k_f J'_{(f+1)f}H_{ff}}, \tag{A.23}$$

with

$$J_{il} = j_n(k_i R_l), \tag{A.24}$$

$$H_{il} = h_n^{(1)}(k_i R_l), \tag{A.25}$$

$$J'_{il} = \frac{1}{\rho}\frac{d[\rho j_n(\rho)]}{d\rho}\bigg|_{\rho=k_i R_l}, \tag{A.26}$$

$$H'_{il} = \frac{1}{\rho}\frac{d[\rho h_n^{(1)}(\rho)]}{d\rho}\bigg|_{\rho=k_i R_l}. \tag{A.27}$$

The coefficients in the first and the last layers can be found immediately from Eqs. (A.13) and (A.14). The rest can be obtained by again using recurrence equations (A.13).

A.2.1 Two-layered medium

For a sphere of radius R (including the special cases of an empty sphere in an otherwise homogeneous medium and a material sphere in vacuum) we have [Li *et al.* (1994)]

$$\begin{aligned} &\boldsymbol{G}^{(11)}(\mathbf{r},\mathbf{r}',\omega) \\ &\quad = \frac{ik_1}{4\pi}\sum_{\substack{e\\o}}\sum_{l=1}^{\infty}\sum_{m=0}^{l}\frac{2l+1}{l(l+1)}\frac{(l-m)!}{(l+m)!}(2-\delta_{0m}) \\ &\quad \times\Big[\mathcal{B}_l^M(\omega)\mathbf{M}^{(1)}_{\substack{e\\o}lm}(\mathbf{r},k_1)\otimes\mathbf{M}^{(1)}_{\substack{e\\o}lm}(\mathbf{r}',k_1) \\ &\quad + \mathcal{B}_l^N(\omega)\mathbf{N}^{(1)}_{\substack{e\\o}lm}(\mathbf{r},k_1)\otimes\mathbf{N}^{(1)}_{\substack{e\\o}lm}(\mathbf{r}',k_1)\Big] \end{aligned} \tag{A.28}$$

$(r, r' > R)$,

$$\begin{aligned} &\boldsymbol{G}^{(22)}(\mathbf{r},\mathbf{r}',\omega) \\ &\quad = \frac{ik_2}{4\pi}\sum_{\substack{e\\o}}\sum_{l=1}^{\infty}\sum_{m=0}^{l}\frac{2l+1}{l(l+1)}\frac{(l-m)!}{(l+m)!}(2-\delta_{0m}) \\ &\quad \times\Big[\mathcal{C}_l^M(\omega)\mathbf{M}_{\substack{e\\o}lm}(\mathbf{r},k_2)\otimes\mathbf{M}_{\substack{e\\o}lm}(\mathbf{r}',k_2) \\ &\quad + \mathcal{C}_l^N(\omega)\mathbf{N}_{\substack{e\\o}lm}(\mathbf{r},k_2)\otimes\mathbf{N}_{\substack{e\\o}lm}(\mathbf{r}',k_2)\Big] \end{aligned} \tag{A.29}$$

$(r, r' < R)$, where

$$\mathcal{B}_l^{M,N}(\omega) = -R_{F1}^{M,N}, \tag{A.30}$$

$$\mathcal{C}_l^{M,N}(\omega) = -R_{F1}^{M,N}\frac{T_{F1}^{M,N}R_{P1}^{M,N}}{T_{P1}^{M,N}}. \tag{A.31}$$

A.2.2 Three-layered medium

For three-layered media of radii R_1 and R_2 ($R_1 > R_2$), the spherical cavity presented in Fig. 4 in particular, we have that [Li *et al.* (1994)]

$$
\begin{aligned}
\boldsymbol{G}^{(13)}(\mathbf{r},\mathbf{r}',\omega) &= \frac{ik_3}{4\pi}\sum_{\substack{e\\o}}\sum_{n=1}^{\infty}\sum_{l=0}^{n} \\
&\times\left\{\frac{2n+1}{n(n+1)}\frac{(n-l)!}{(n+l)!}(2-\delta_{0l})\right. \\
&\times\left[\mathcal{A}_l^M(\omega)\mathbf{M}^{(1)}_{\substack{e\\o}nl}(\mathbf{r},k_1)\otimes\mathbf{M}_{\substack{e\\o}nl}(\mathbf{r}',k_3)\right. \\
&\left.\left.+\mathcal{A}_l^N(\omega)\mathbf{N}^{(1)}_{\substack{e\\o}nl}(\mathbf{r},k_1)\otimes\mathbf{N}_{\substack{e\\o}nl}(\mathbf{r}',k_3)\right]\right\} \qquad \text{(A.32)}
\end{aligned}
$$

$(r < R_2,\ r' > R_1)$,

$$
\begin{aligned}
\boldsymbol{G}^{(33)}(\mathbf{r},\mathbf{r}',\omega) &= \frac{ik_3}{4\pi}\sum_{\substack{e\\o}}\sum_{n=1}^{\infty}\sum_{l=0}^{n} \\
&\times\left\{\frac{2n+1}{n(n+1)}\frac{(n-l)!}{(n+l)!}(2-\delta_{0l})\right. \\
&\times\left[\mathcal{C}_l^M(\omega)\mathbf{M}_{\substack{e\\o}nl}(\mathbf{r},k_1)\otimes\mathbf{M}_{\substack{e\\o}nl}(\mathbf{r}',k_3)\right. \\
&\left.\left.+\mathcal{C}_l^N(\omega)\mathbf{N}_{\substack{e\\o}nl}(\mathbf{r},k_1)\otimes\mathbf{N}_{\substack{e\\o}nl}(\mathbf{r}',k_3)\right]\right\} \qquad \text{(A.33)}
\end{aligned}
$$

$(r,\ r' > R_1)$, where

$$
\mathcal{A}_l^{M,N}(\omega)=\frac{T_{F1}^{M,N}T_{F2}^{M,N}T_{P1}^{M,N}}{T_{P1}^{M,N}+T_{F1}^{M,N}R_{P1}^{M,N}R_{F2}^{M,N}}\,, \qquad \text{(A.34)}
$$

$$
\mathcal{C}_l^{M,N}(\omega)=\frac{\mathcal{A}_l^{M,N}}{T_{P2}^{M,N}}\left[\frac{R_{P2}^{M,N}}{T_{F1}^{M,N}}+\frac{R_{P1}^{M,N}}{T_{P1}^{M,N}}\right]. \qquad \text{(A.35)}
$$

References

Abrikosov, A.A., Gorkov, L.P., and Dzyaloshinski, I.E. 1975, Methods of Quantum Field Theory in Statistical Physics, Dover, New York.

Agarwal, G.S. 1975, Phys. Rev. A, 12, 1475.

Agarwal, G.S., and Gupta, S.D. 1998, Phys. Rev. A, 57, 667.

Agarwal, G.S., and Gupta, S.D. 2000, e-print quant-ph/0011098.

Agarwal, G.S and ONeil, S.V. 1983, Phys. Rev. B, 28, 487.

Agarwal, G.S., and Vollmer, H.D. 1977, Phys. Stat. Sol. B, 79, 249.

Andrew, P., and Barnes, W.L. 2000, Science, 290, 785.

Barnes, M.D., Kung, C-Y., Whitten, W.B., Ramsey, J.M., Arnold, S., and Holler, S. 1996, Phys. Rev. Lett., 76, 3931.

Barnett, S.M., Huttner, B., and Loudon, R. 1992, Phys. Rev. Lett., 68, 3698.

Barnett, S.M., Huttner, B., Loudon, R., and Matloob, R. 1996, J. Phys. B, 29, 3763.

Bay, S., Lambropoulous, P., and Mølmer, K. 1997, Phys. Rev. A, 55, 1485.

Beige, A., Munro, W.I., and Knight, P.L. 2000, Phys. Rev. A, 62, 052102.

Bell, J.S. 1965, Physics 1, 195.

Berman, P.R. (Ed.) 1994, Cavity Quantum Electrodynamics, Academic, New York.

Betzig, E., and Chichester, R.J. 1993, Science, 262, 1422.

Bian, R.X., Dunn, R.C., Xie, X.S., and Leung, P.T. 1995, Phys. Rev. Lett., 75, 4772.

Chance, R.R., Prock, A., and Silbey, R. 1978, Advances in Chemical Physics 37, I. Prigogine and S.A. Rice (Eds.), Wiley, New York, 1.

Chang, R.K., and Campillo, A.J. (Eds.) 1996, Optical Processes in Microcavities, World Scientific, Singapore.

Chew, H. 1987, J. Chem. Phys., 87, 1355.

Chew, W.C. 1995, Waves and Fields in Inhomogeneous Media, IEEE Press, New York.

Ching, S.C., Lai, H.M., and Young, K. 1987, J. Opt. Soc. Am. B, 4, 2004.

Cirac, J.I., and Zoller, P. 1994, Phys. Rev. A, 50, R2799.

Clauser, J.F., Horne, M.A., Shimony, A., and Holt, R.A. 1969, Phys. Rev. Lett., 23, 880.

Collot, L., Lefèvre-Seguin, V., Brune, M., Raimond, J.M., and Haroche, S. 1993, Euro. Phys. Lett., 23, 327.

Cook, R.J., and Milonni, P.W. 1987, Phys. Rev. A, 35, 5081.

Crenshaw, M.E., and Bowden, C.M. 2000a, Phys. Rev. Lett., 85, 1851.

Crenshaw, M.E., and Bowden, C.M. 2000b, Phys. Rev. A, 63, 013801.

De Martini, F., and Jacobovitz, G.R. 1988, Phys. Rev. Lett., 60, 1711.

De Martini, F., Di Giuseppe, G., and Marrocco, M. 1996, Phys. Rev. Lett. 76, 900.

De Voe, R.G., and Brewer, R.G. 1996, Phys. Rev. Lett., 76, 2049.

de Vries, P., and Lagendijk, A. 1998, Phys. Rev. Lett., 81, 1381.

Dexter, D.L. 1956, Phys. Rev., 101, 48.

di Bartolo, B. 1968, Optical Interactions in Solids, Wiley, New York.

Drexhage, K.H. 1974, Progess in Optics XII, E. Wolf (Ed.), North-Holland, Amsterdam, 165.

Druger, S.D. , Arnold, S., and Folan, L.M. 1987, J. Chem. Phys., 87, 2649.

Feng, X.P., and Ujihara, K. 1989, IEEE J. Quantum Electron., QE-25, 2332.

Fichet, M., Schuller, F., Bloch, D., and Ducloy, M. 1995, Phys. Rev. A, 51, 1553.

Fleischhauer, M. 1999, Phys. Rev. A, 60, 2534.

Folan, L.M., Arnold, S., and Druger, S.D. 1985, Chem. Phys. Lett., 118, 322.

Freyberger, M., Aravind, P.K., Horne, M.A., and Shimony, A. 1996, Phys. Rev. A, 53, 1232.

Fujiwara, H., Sasaki, K., and Masuhara, H. 1999, J. Appl. Phys., 85, 2052.

Gerry, C.C. 1996, Phys. Rev. A, 53, 2857.

Gersen, H., García-Parajó, M.F., Novotny, L., Veerman, J.A., Kuipers, L., and van Hulst, N.F. 2000, Phys. Rev. Lett., 85, 5312; see also references therein.

Gersten, J. I., and Nitzan, A. 1984, Chem. Phys. Lett., 104, 31.

Glauber, R.J., and Lewenstein, M. 1991, Phys. Rev. A, 43, 467.

Goldstein, E.V., and Meystre, P. 1997a, Phys. Rev. A, 56, 5135.

Goldstein, E.V., Pax, P., and Meystre, P. 1997b, Phys. Rev. A, 53, 2604.

Gorodetsky, M.L., Savchenkov, A.A, and Ilchenko, V.S. 1996, Opt. Lett., 21, 453.

Gruner, T., and Welsch, D.-G. 1996, Phys. Rev. A, 53, 1818.

Guzmán, A.M., and Meystre, P. 1998, Phys. Rev. A, 57, 1139.

Hagley, E., Maitre, X., Nogues, G., Wunderlich, C., Brune, M., Raimond, J.M., and Haroche, S. 1997, Phys. Rev. Lett., 79, 1.

Haroche, S. 1992, Fundamental Systems in Quantum Optics, J. Dalibard, J.-M. Raimond, and J. Zinn-Justin (Eds.), North-Holland, Amsterdam, 767.

Haroche, S. 1998, Phys. Script., 76, 159.

Henkel, C., and Sandoghdar, V. 1998, Opt. Commun., 158, 250.

Hinds, E.A. 1991, Advances in Atomic, Molecular, and Optical Physics, D. Bates and B. Bederson (Eds.), Academic, New York, 28, 237.

Ho, S.-T., and Kumar, P. 1993, J. Opt. Soc. Am. B, 10, 1620.

Ho Trung Dung, and Ujihara, K. 1999, Phys. Rev. A, 60, 4067.

Ho Trung Dung, Knöll, L., and Welsch, D.-G. 1998, Phys. Rev. A, 57, 3931.

Ho Trung Dung, Knöll, L., and Welsch, D.-G. 2000, Phys. Rev. A, 62, 053804.

Ho Trung Dung, Knöll, L., and Welsch, D.-G. 2001, Phys. Rev. A, in press, (e-print quant-ph/0012103).

Hopmeier, M., Guss, W., Deussen, M., Göbel, E.O., and Mahrt, R.F. 1999, Phys. Rev. Lett., 82, 4118.

Hunt, N.E.J., Schubert, E.F., Kopf, R.F., Sivco, D.L., Cho, A.Y., and Zydzik, G.J. 1993, Appl. Phys. Lett., 63, 2600.

Huttner, B., and Barnett, S.M. 1992, Phys. Rev. A, 46, 4306.

Joannopoulous, J.D., Meade, R.D., and Winn, J.N. 1995, Photonic Crystals, Princeton, New York.

John, S. 1987, Phys. Rev. Lett., 58, 2486.

John, S., and Wang, J. 1991, Phys. Rev. B, 43, 12772.

John, S., and Quang, T. 1994, Phys. Rev. A, 50, 1764.

John, S., and Quang, T. 1995, Phys. Rev. A, 52, 4083.

Juzeliūnas, G. 1997, Phys. Rev. A, 55, R4015.

Juzeliūnas, G., and Andrews, D.L. 1994a, Phys. Rev. B., 49, 8751.

Juzeliūnas, G., and Andrews, D.L. 1994b, Phys. Rev. B., 50, 13371.

Khitrova, G., Gibbs, H.M., Jahnke, F., Kira, M., and Koch, S.W. 1999, Rev. Mod. Phys., 71, 1591.

Kimble, H.J. 1998, Phys. Script. 76, 127.

Kitson, S.C., Jonsson, P., Rarity, J.G., and Tapster, P.R. 1998, Phys. Rev. A, 58, 620.

Kleppner, D. 1981, Phys. Rev. Lett., 47, 233.

Klimov, V.V., Ducloy, M., and Letokhov, V.S. 1996, J. Mod. Opt., 43, 2251.

Knoester, J., and Mukamel, S. 1989, Phys. Rev. A, 40, 7065.

Knöll, L., and Welsch, D.-G. 1992, Prog. Quant. Electr., 16, 135.

Knöll, L., Scheel, S., and Welsch, D.-G. 2001 (in press), Coherence and Statistics of Photons and Atoms, J. Perina (Ed.), John Wiley & Son, New York (e-print quant-ph/0006121).

Kobayashi, T., Zheng, Q., and Sekiguchi, T. 1995a, Phys. Rev. A, 52, 2835.

Kobayashi, T., Zheng, Q., and Sekiguchi, T. 1995b, Phys. Lett. A, 199, 21.

Kofman, A.G., Kurizki, G., and Sherman, B. 1994, J. Mod. Opt., 41, 353.

Kopelman, R., and Tan, W. 1993, Science, 262, 1382.

Kudryavtsev, I.K., and Knight, P.L. 1993, J. Mod. Opt., 40, 1673.

Kurizki, G., and Genack, A.Z. 1988, Phys. Rev. Lett., 61, 2269.

Kurizki, G. 1990, Phys. Rev. A, 42, 2915.

Kurizki, G., Kofman, A.G., and Yudson, V. 1996, Phys. Rev. A, 53, R35.

Kuzmich, A., Walmsley, I.A., and Mandel, L. 2000, Phys. Rev. Lett., 85, 1349; and references therein.

Lai, H.M., Leung, P.T., and Young, K. 1988, Phys. Rev. A, 37, 1597.

Lee, Y., and Yamanishi, M. 1995, Phys. Rev. A, 52, 2312.

Lermer, N., Barnes, M.D., Kung, C-Y., Whitten, W.B., Ramsey, J.M., and Hill, S.C. 1998, Opt. Lett., 23, 951.

Leung, P.T., and Young, K. 1988, J. Chem. Phys., 89, 2894.

Lewenstein, M., Zakrzewski, J., Mossberg, T.W., and Mostowski, J. 1988a, J. Phys. B, 21, L9.

Lewenstein, M., Zakrzewski, J., and Mossberg, T.W. 1988b, Phys. Rev. A, 38, 808.

Li, L.W., Kooi, P.S., Leong, M.S., and Yeo, T.S. 1994, IEEE Trans. Microwave Theory Tech., 42, 2302.

Lin, H-B., Eversole, J.D., Merritt, C.D., and Campillo, A.J. 1992, Phys. Rev. A, 45, 6756.

Loudon, R. 1983, Quantum Theory of Light, Oxford University Press, Oxford.

Maradudin, A.A., and Mills, D.L. 1975, Phys. Rev. B, 11, 1392.

Matloob, R., Loudon, R., Barnett, S.M., and Jeffers, J. 1995, Phys. Rev. A, 52, 4823.

Matloob, R., and Loudon, R. 1997, Phys. Rev. A, 53, 4567.

Matloob, R. 2000, Phys. Rev. A, 61, 062103.

Meschede, D. 1992, Phys. Rep., 211, 201.

Meschede, D., Jhe, W., and Hinds, E.A. 1990, Phys. Rev. A, 41, 1587.

Meystre, P. 1992, Progress in Optics, E. Wolf (Ed.), North-Holland, Amsterdam, 30.

Mills, D.L., and Maradudin, A.A. 1975, Phys. Rev. B, 12, 2943.

Milonni, P.W. 1995, J. Mod. Opt., 42, 1991.

Nienhuis, G., and Alkemade, C.Th.J. 1976, Physica C, 81, 181.

Nikolopoulos, G.M., and P. Lambropoulos, P. 2000, Phys. Rev. A, 61, 053812.

Peres, A. 1996, Phys. Rev. Lett., 77, 1413.

Phoenix, S.J.D., and Barnett, S.M. 1993, J. Mod. Opt., 40, 979.

Plenio, M.B.,Huelga, S.F., Beige, A., and Knight, P.L. 1999, Phys. Rev. A, 59, 2468.

Protsenko, I., Domokos, P., Lefèvre-Seguin, V., Hare, J., Raimond, J.M., and Davidovich, L. 1999, Phys. Rev. A, 59, 1667; see also references therein.

Purcell, E.M. 1946, Phys. Rev., 69, 681.

Raether, H. 1988, Surface Plasmons on Smooth and Rough Surfaces and on Gratings, Springer-Verlag, Berlin.

Rikken, G.L.J.A., and Kessener, Y.A.R.R. 1995, Phys. Rev. Lett., 74, 880.

Rowe, M.A., Kielpinski, D., Meyer, V., Sackett, C.A., Itano, W.M., Monroe, C., and Wineland, D.J. 2001, Nature, 409, 791.

Rupasov, V., and Singh, M. 1997, Phys. Rev. A, 56, 898.

Ruppin, R. 1982, J. Chem. Phys., 76, 1681.

Sachdev, S. 1984, Phys. Rev. A, 29, 2627.

Scheel, S., Knöll, L., and Welsch, D.-G. 1998, Phys. Rev. A, 58, 700.

Scheel, S., Knöll, L., Welsch, D.-G., and Barnett, S.M. 1999a, Phys. Rev. A, 60, 1590.

Scheel, S., Knöll, L., and Welsch, D.-G. 1999b, Phys. Rev. A, 60, 4094.

Scheel, S., Knöll, L., and Welsch, D.-G. 1999c, Acta Phys. Slov., 49, 585.

Schriemer, H.P., van Driel, H.M., Koenderink, A.F., and Vos, W.L. 2001, Phys. Rev. A, 63, 011801(R); see also references therein.

Schuurmans, F.J.P., de Lang, D.T.N., Wegdam, G.H., Sprik, R., and Lagendijk, A. 1998, Phys. Rev. Lett., 80, 5077.

Soukoulis, C.M. (Ed.) 1996, Photonic Band Gap Materials, Kluwer, Dordrecht.

Tai, C.-T. 1994, Dyadic Green Functions in Electromagnetic Theory, IEEE Press, New York.

Tip, A. 1998, Phys. Rev. A, 57, 4818.

Tip, A., Knöll, L., Scheel, S., and Welsch, D.-G. 2001, Phys. Rev. A., 63, 043806.

Tomaš, M.S. 1995, Phys. Rev. A, 51, 1347.

Tomaš, M.S. 2001, Phys. Rev. A, in press, (e-print quant-ph/0009057).

Tomaš, M.S., and Lenac, Z. 1999, Phys. Rev. A, 60, 2431.

Uetake, S., Katsuragawa, M., Suzuki, M., and Hakuta, K. 1999, Phys. Rev. A, 61, 011803.

Vaidman, L. 2001, e-print quant-ph/0102139.

Vernooy, D.W., Furusawa, A., Georgiades, N.Ph., Ilchenko, V.S., and Kimble, H.J. 1998a, Phys. Rev. A, 57, R2293.

Vernooy, D.W., Ilchenko, V.S., Mabuchi, H., Streed, E.W., and Kimble, H.J. 1998b, Opt. Lett., 23, 247.

Vogel, W., and Welsch, D.-G. 1994, Lectures on Quantum Optics, Akademie Verlag, Berlin, Germany, 212.

Walther, H. 1998, Phys. Script., 76, 138.

Weihs, G., Jennewein, T., Simon, C., Weinfurter, H., and Zeilinger, A. 1998, Phys. Rev. Lett., 81, 5039.

Woldeyohannes, M., and John, S. 1999, Phys. Rev. A, 60, 5046.

Wubs, M., and Suttorp, L.G. 2001, Phys. Rev. A, 63, 043809.

Wylie, J.M., and Sipe, J.E. 1984, Phys. Rev. A, 30, 1185.

Wylie, J.M., and Sipe, J.E. 1985, Phys. Rev. A, 32, 2030.

Yablonovich, E. 1987, Phys. Rev. Lett., 58, 1059.

Yamamoto, Y., and Slusher, R.E. 1993, Phys. Today, June, 66.

Yamamoto, Y., Tassone, F., and Cao, H. 2000, Semiconductor Cavity Quantum Electrodynamics, Springer, Berlin.

Yariv, A. 1975, Quantum Electronics, Wiley, New York.

Yeung M.S., and Gustafson, T.K. 1996, Phys. Rev. A, 54, 5227.

Yokoyama, H., and Ujihara. K (Eds.) 1995, Spontaneous Emission and Laser Oscillation in Microcavities, CRC Press, Boca Raton.

Yukawa, H., Arnold, S., and Miyano, K. 1999, Phys. Rev. A, 60, 2491.

Zhu, S.Y., Yang, Y., Chen, H., Zheng, H., and Zubairy, M.S. 2000, Phys. Rev. Lett., 84, 2136.